LAWRENCE
LIVERMORE
NATIONAL
LABORATORY

UCRL-TR-210934

Design of 3x3 focusing array for heavy ion driver. Final report on CRADA

N. N. Martovetsky

March 30, 2005

This work was performed under the auspices of the U.S. Department of Energy by University of California, Lawrence Livermore National Laboratory under Contract W-7405-Eng-48.

LLNL

Memo

To: Rainer Meinke, AML

From: Nicolai Martovetsky

CC: Distribution

Date: 03/25/2005

Re: Design of 3x3 focusing array for heavy ion driver. Final report on CRADA

Inv. # 2004ADVN3121.

Agreement ID 1020484.

Funding agreement TC-02082-04.

Proposal M10429.

Table of contents

Executive summary

This memo presents a design of a 3x3 quadrupole array for HIF. It contains 3 D magnetic field computations of the array build with racetrack coils with and without different shields. It is shown that it is possible to have a low error magnetic field in the cells and shield the stray fields to acceptable levels. The array design seems to be a practical solution to any size array for future multi-beam heavy ion fusion drivers.

Introduction

This work is a logical continuation of the work [1], where it was shown that focusing arrays made with racetracks look promising in 2D analysis. The work [1] was inspired by work [2], but in [2] there was no practical solution for the termination coils. It was shown in [1] that in the 2D geometry it is possible to create a quadrupole field with racetrack coils with an error on the level of several units of 1e-4 and with relatively low stray field. The analysis performed in [1] studied only two components of the error field, namely a6 and a10 (six poles and twenty poles), because due to symmetry only 6, 10, 14, 18, etc harmonics exist in a single quadrupole, and higher than 10th harmonics are negligibly small at the aperture of the radius 2/3 of the cell size or smaller. The 2/3 radius of the cell is a "rule-of-thumb" size of the beam. At larger radius the higher harmonics are becoming large, but since this area is not available for the beam, it is not important, so we pay little attention to higher harmonics in this problem. However, in contrast to a single quadrupole, in the array cells, the other harmonics are present and needed to be analyzed and reduced as necessary.

It was decided by the HIF program, that to demonstrate the feasibility of the concept we need to design, build and test a representative array, which was agreed by the HIF community to be 3x3.

We need to develop termination magnets, which would do two things:

1. Leave the quadrupole field inside the bores of a finite array the same as it would have been in the infinite array
2. Have no stray field outside the array.

The magnet design should be relevant to bigger arrays, like 5x5 or 10x10, since 3x3 array serves as a proof of principle for larger arrays for HIF driver.

Requirements

The set of requirements is given in Table 1.

Table 1. Specifications for the Quadrupole Array SBIR

10/17/04

Basic design specifications:

Number of channels:	9		(fixed)
Clear bore radius:	30	mm	(fixed)
Cell half-size:	40	mm	(optimize)
Physical coil length:	600	mm	(fixed)
Total physical length:	350	mm	(optimize)
Short sample gradient:	85	T/m	(optimize)
Operating current:	$0.7*I_{ss}$		(fixed)
Operating temperature:	4.5	K	(fixed)
Copper current density:	1.5 kA/mm^2 @ I_{ss}		(fixed)
Magnetic length:	57	cm	(optimize)
Harmonics Ref. Radius:	17	mm	(fixed)
Field quality:	< 50 units @ I_{op}		(optimize)

Training:

- First quench above 80% I_{ss}
- Reach 95% I_{ss} in 5 quenches
- First quench above 95% I_{ss} after a thermal cycle.

Notes:

Geometric specs apply to the cold mass only, no specs on the cryostat at this point.

I would assume a cold bore design where the minimum clear bore radius given applies to the inside surface of the liner (LHC-type design). In a warm bore version using the same coils, the clear bore would probably end up being smaller. Note the clear bore definition is different from HCX-MAG-01-0222-01. In that case, we had just specified the inner radius of the structure.

The total physical length includes coil, structure, joints/leads and their support.

The total radial buildup includes flux termination and mechanical support structure.

I_{ss} is the "conductor limited" quench current or "short sample current". This choice results in an operating gradient of about 60 T/m for the target short sample gradient of 85 T/m.

Detailed field error and magnetic length definitions and formulas are given in the note "Characterization of Prototype Superconducting Magnetic Quadrupoles for the High Current Transport Experiment", Lund et al., February 22, 2001, available on the HCX server HCX-MAG-01-0222-01. A reference coordinate system is also defined.

Transverse leakage flux: an ideal, circular magnetic boundary outside the array, with a radius of 230 mm and off-centered by 1 cm with respect to the array center will not cause the field errors to go outside the specified range in any of the cells.

Longitudinal leakage flux: Quadrupole gradient at I_{op} drops to less than 5 T/m within 4 cm from the physical edge of the coil (optimize).

Design optimization/Figures of merit:

Assuming that the basic geometric and magnetic specs can be met, further design optimization should seek:

- Higher gradient
- Larger clear bore
- Lower field errors
- Higher magnetic length
- Smaller total physical length
- Smaller radial buildup
- Faster longitudinal field decay

We should assign some relative weight to the different optimization targets.

Note that the requirements for the field quality were intentionally loose (50 units), since so far there was no baseline design that would have shown what was possible and reasonable and what was not. An agreement between the HIF experts is that it would be desirable to have 10 units error field average.

There are some implicit requirements of a practical nature, which are not spelled out.

Needless to say that one of the most important requirement is the minimum cost, which implies minimum of spacers and non-standard elements.

There are no requirements for the peak field either, but we assume that it would be very undesirable to have a peak field just in one local area which would be significantly higher than the peak fields in other coils; we will try to avoid that.

Also, we assume that all conductors are charged in series to one power supply.

There are not many specs on the stray field, but it is known that the induction accelerator core is made out of a ferromagnetic material; therefore the level of magnetic field shall be not much higher than a natural Earth magnetism (about 0.5 G). We assume that it should be below 10 G in places where these cores could be installed (outside of the cryostat, several centimeters away, TBD).

The other constraints come from the selection of the conductor and structure.

For our studies we will adopt the following design choices:

1. Cable used in previous R&D – bare 1.17x4.05mm, in insulation 1.35x4.4 mm.
2. Minimum cable bend radius – 8 mm
3. Flat racetracks geometry
4. Winding pack is at least 3 mm from the corner
5. 36 mm cell size

Requirement 4 has to do with the allowance for the structural material that will support the forces during fabrication. In the previous prototypes it was demonstrated that a large prestress of the winding pack eliminates the degradation and makes training non-existent or very quick. The distance of the winding pack from the corner is shown in Fig. 1 by a line with two diamonds and denoted as "d".

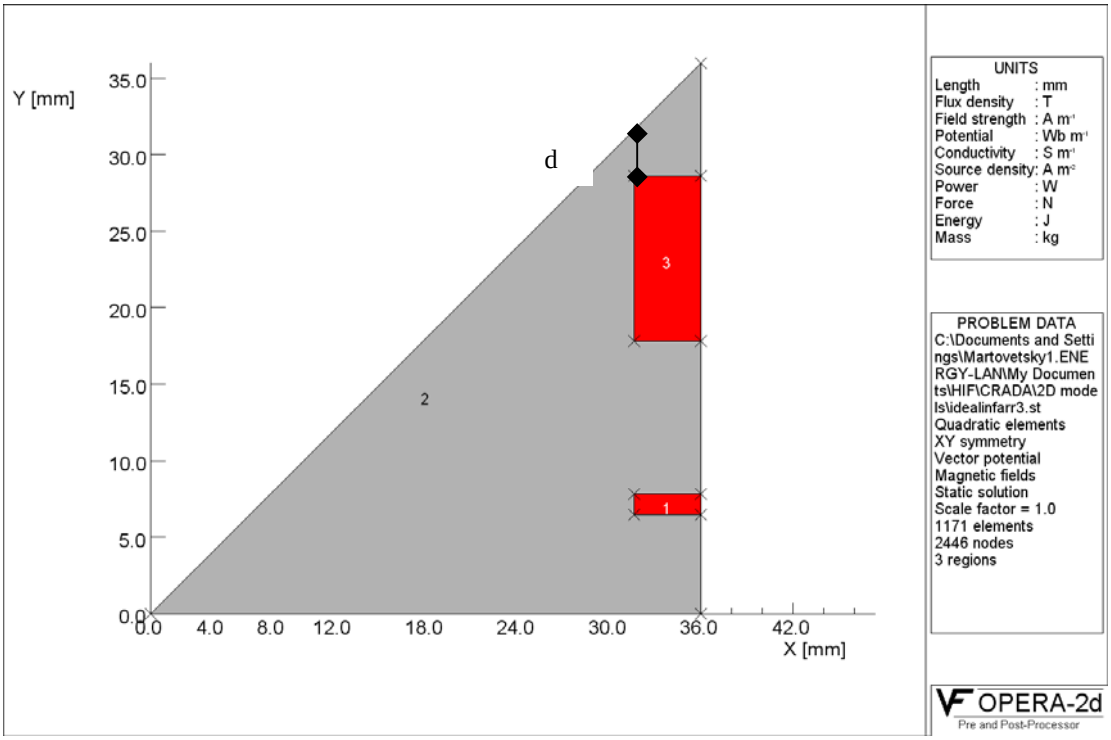

Fig. 1. An acceptable solution of the winding for an infinite array. The winding (areas 1 and 3) are separated by an optimized gap.

This distance from the corner is related to a structure, which provides prestress. The thickness of this structure is 1.6 mm, which is a result of the selected winding-to-winding clear bore of 60 mm (30 mm per side), 72 mm cell size (36 mm per side) and the conductor height of 4.4 mm.

In the array the forces acting in the corner are balanced by other cells, so the corner is in balanced compression, therefore there will be no net force to support from the winding pack in operation for inner pancakes. The outer pancakes, or shielding pancakes will require some structural support and that will be supported by some kind of outside band, which may be a helium container holding the array, as it was done in the prototype cryostat recently designed and built in collaboration by LLNL and MIT [3].

Design development plan

Our plan of developing the 3x3 array design is the following.

First, we will find a solution in 2D geometry for the infinite array within our constrains, which will have minimal practical error field and would be achievable. Initial point of the design is the solution proposed in [1].

Second, we will try to simplify the winding arrangement without too much increase in the error and stray fields.

Third, we will try to improve the field quality in the cell by manipulating the shielding windings (to see how much freedom we have in doing this).

Forth, we will build a 3D model and explore how much end effects contribute to the integrated error field and stray fields.

Fifth, we will study the stray field and attempt to reduce it to an acceptably low level by introducing an iron shield.

Infinite array

We start with an infinite array and find the configuration of the windings, which will have the minimal error field harmonics. From the symmetry, only a2, a6, a10, a14… are non-zero, but at R=20, a14, and higher harmonics are small. With our constraints we could not find a solution, which would provide low a6 and a10 harmonics $(a_6^2 + a_{10}^2)^{1/2}$ <1e-3 at R=20 mm with the continuous winding with no gaps.

The calculations are done for 500 A/mm^2 in the winding pack, which is achievable for this conductor we chose to do the analysis with, as it was confirmed in the previous R&D. The maximum achievable current density will be determined later by the Ic(B) curve and the peak field load line later in this memo. By trial and error we have found a solution, which satisfy the low error field criteria. The geometry of the windings is shown in Fig. 1. The y-coordinates of the conductors are as follows: one turn, 1.35 mm thick starts at y=7.45 mm, then after a 9 mm-wide gap the winding pack denoted as

3 starts at y=17.8 mm and spans to y= 28.6 mm, which is 8 turns, so there are 9 turns of the 1.35 mm thick conductor in the single pancake winding pack.

The harmonics of the field for such an infinite array are given in Table 2.

Table 2. Harmonics in the infinite array with 3 mm corner space.

Harmonics @ R=20 mm	Value, T
b2	-1.05
b6	5.3e-4
b10	1.9e-4
b14	-6.5e-5

As we can see from the table, the gradient is b2/20e-3=52.5 T/m at 500 A/mm2. Also harmonic b2 is close enough to 1, so other harmonics could be evaluated in T, instead of relative harmonics b6/b2, etc.

Let us make a deviation from our baseline design assumption of 3 mm (constraint No. 4 in the list of constrains above) and see how much advantage we would have had with this design if we would allow a smaller space for the structure. We assume that 2 mm could be feasible. We have found an optimum geometry for such a case when the error field harmonics to be within allowable 1e-3. The y-coordinates of the conductors are as follows: one turn 1.35 mm thick starts at y=5.3 mm, the winding pack denoted as 3 in Fig. 1 starts at y=16.1 mm and spans to 29.6 mm which leaves 2 mm to the end of the structure. That makes total amount of turns 11 and helps in increasing the gradient.

The results of this optimization in terms of the field is given in Table 3.

Table 3. Harmonics in the infinite array with 2 mm corner space.

Harmonics @ R=20 mm	Value, T
b2	-1.27
b6	1.4e-4
b10	3.26e-4
b14	-2.3e-5

As we can see, there is a solution for 2 mm, which with about the same error field gives about 20% more powerful gradient.

Like in the previous case of 3 mm in the corner, the optimum version with 2 mm in the corner does not allow having complete cancellation of the a6 and a10 harmonics with one gap. Another gap

is needed, but I did not pursue that since the error field is low enough. Earlier, Rainer Meinke [4] showed that it was possible to find a solution for complete cancellation of the b6 and b10 harmonics with one gap, but he was not constrained with any particular width of the cable assuming full flexibility in this choice. So it seems from his results that it may be possible to improve that, but in the solution given in [4], winding packs do not contain integer number of turns, unless the conductors are made extremely thin. Thus, it looks like the realistic conductor width may be a real constraint on the way to a lower error field.

This ends our deviation from the baseline design with 3 mm space to the 2 mm space version, and we return back to the 3 mm space constraint.

On the basis of the solution in Fig. 1 we will design the 3x3 array in 2 D, which is compatible with the principles given in [1]. The design of the idealized array with the lump windings is shown in Fig. 2.

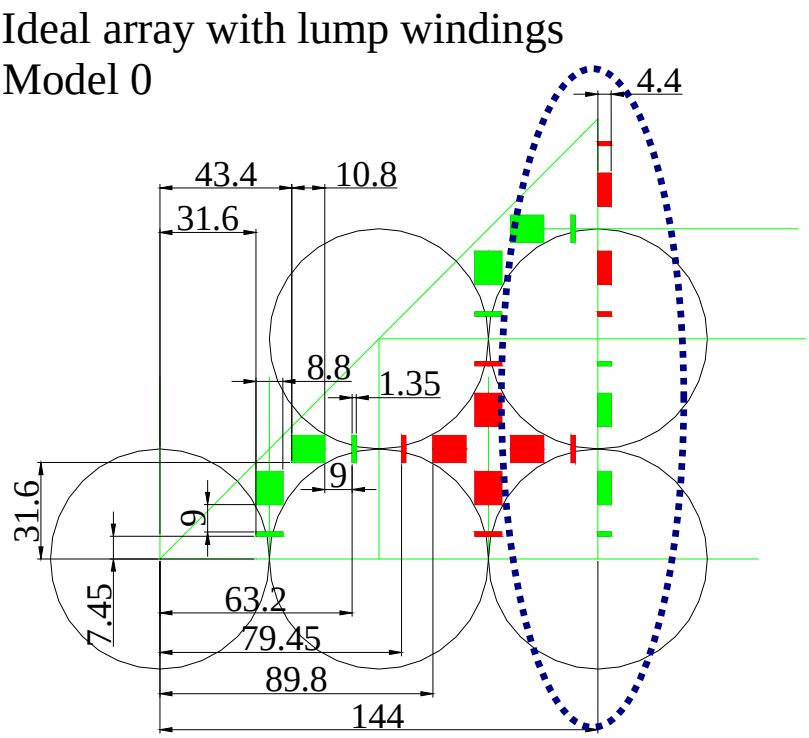

Fig. 2. Geometry of the initial Model 0, dimensions are in mm. Red color corresponds to currents flowing in opposite direction than that in the green colored winding packs. For example, if red colored winding packs have current flowing towards us, the green ones have the current flowing away from us.

One can see that all the winding are the same pancake windings as for the infinite array, except the shielding windings encircled by an oval in Fig.2. We will call the shielding windings all the windings in Fig. 2 with x>108 mm, excluding those windings which are attached to this axis. I encircled these winding packs with an ellipse. We refer the windings at x=144 mm as the “outmost” shielding, while the windings from the previous layer we will call “inner” shielding windings. As one can see in Fig. 2 the inner shielding windings are not racetracks. We will try to change that in the following modifications.

Originally without too much thinking we placed the shielding windings starting at x=144 mm. A more symmetrical position of these 4.4 mm thick windings would be starting at 141.8 mm, since then the center line of the windings would be on the axis of the symmetry at x=144.

Indeed, this corrected model is shown in Fig. 3 and is called the Model 1. The field quality did not change much, but the stray field is noticeably better in the Model 1.

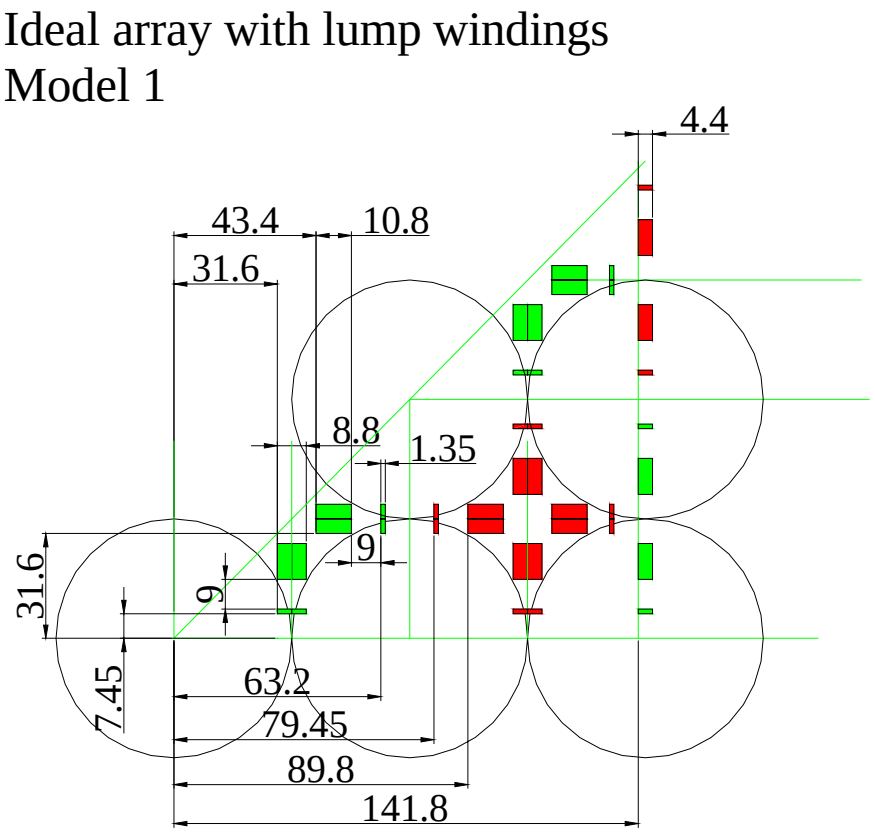

Fig. 3. Improved Model 1.

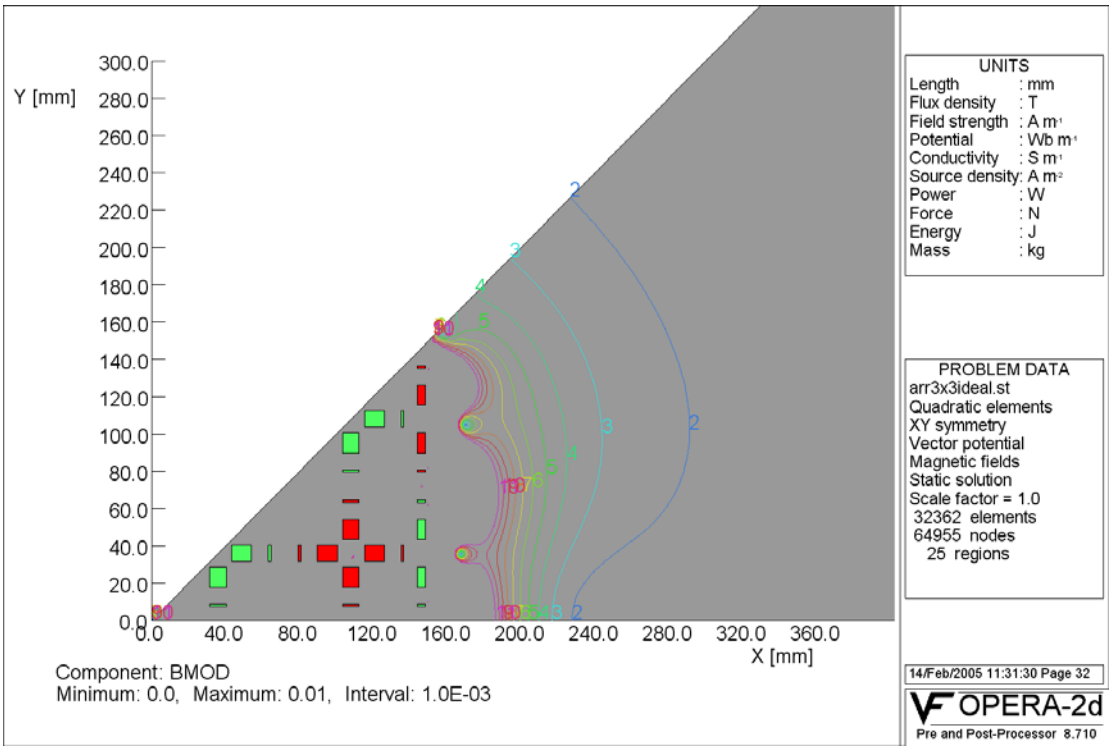

Fig. 4. Model 0 stray field. Line 2 corresponds to 10 G, line 3 to 20 G and so forth.

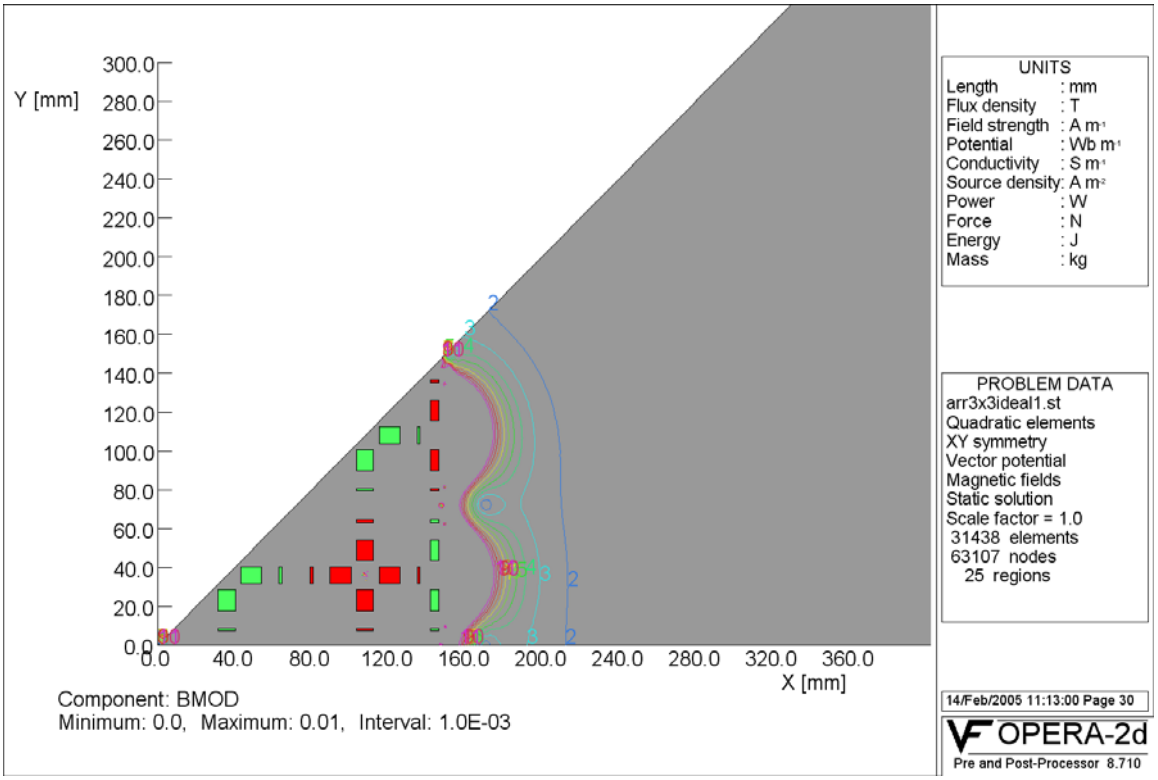

Fig. 5. Model 1 stray field.

As indicated in Fig. 4 and 5, stray field of Model 0 and Model 1 shows that it is very sensitive to the location of the outer shielding racetracks.

The next modification we did to simplify the windings is the iteration 2a, shown in Fig. 6.

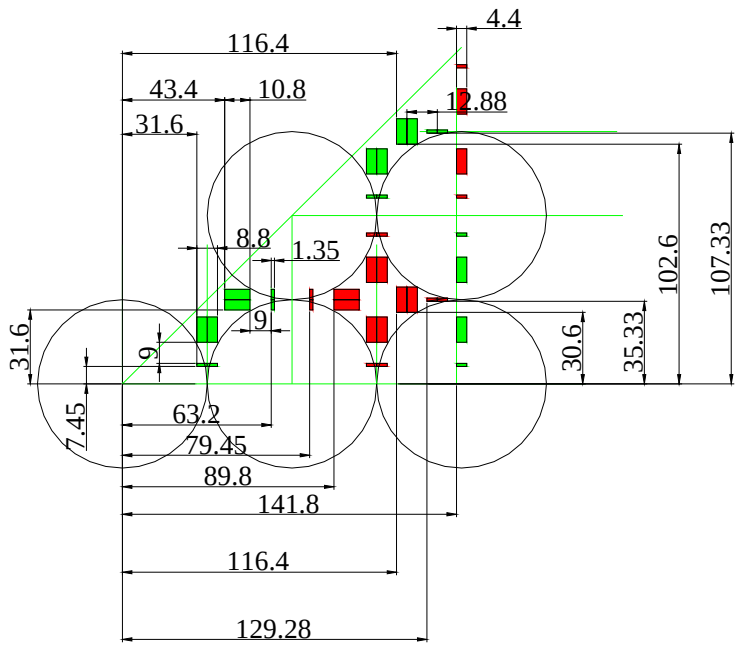

Fig. 6. Model 2a.

We called it the Model 2a since the Model 2 had a slight error and is not discussed here.

We rotated the windings of the inner shields to turn them into two separate double pancakes. The center of rotation was naturally the center of gravity of these winding packs. By doing this we obtain a windable geometry, all of the coils are pancakes (all windings except outer shields are double pancakes, while the outer shields are single pancakes).

The next modification we made was merging the windings in the inner shielding level to convert two independent pancakes into one set. We did this merge again preserving the center of gravity of these windings. The resulting geometry we call the Model 3; it is shown in Fig. 7.

Ideal array with lump windings
Model 3 - merge some shielding windings

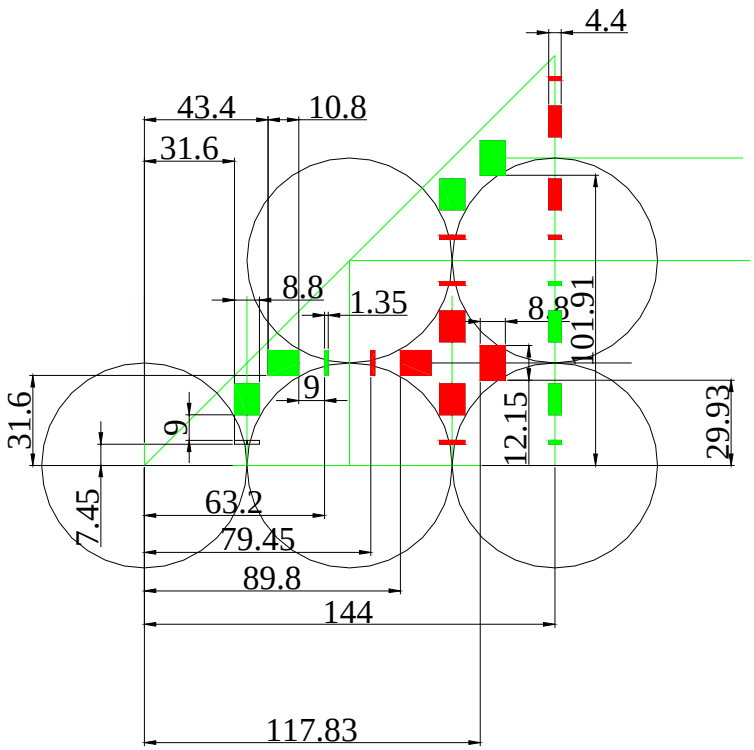

Fig.7. The Model 3 geometry

In the next iteration we merged windings in the outmost shielding windings, again preserving the center of gravity of the merging winding packs. The result is shown in Fig. 8.

Ideal array with lump windings
Model 4 - merge more shielding windings

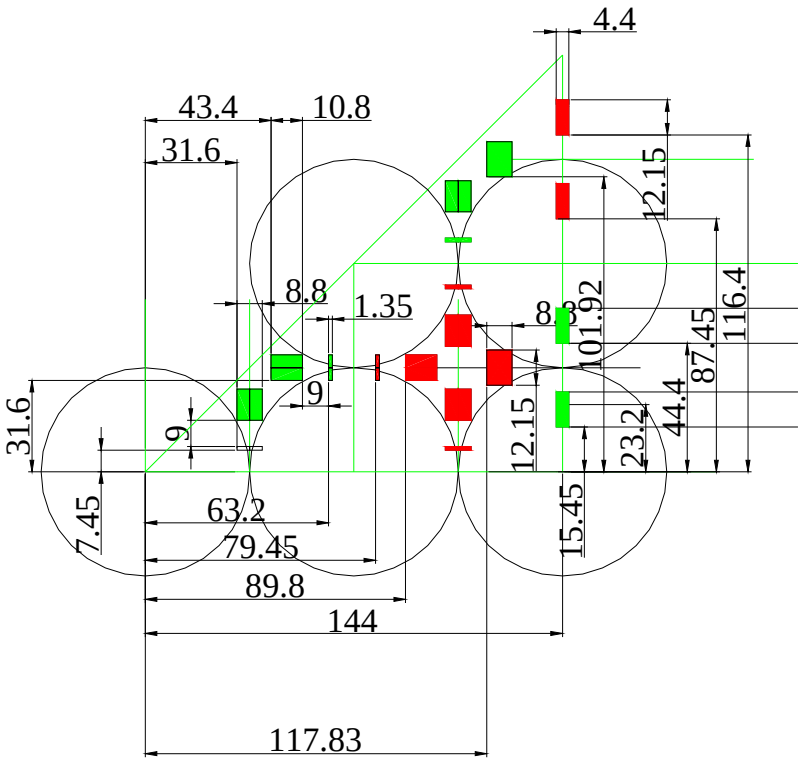

Fig. 8. Model 4.

Here we have significantly simplified windings and the error field (discussed later) still looks acceptable. This Model 4 can be modified further to a model 4A, which contains only double pancakes. Such a configuration is shown in Fig. 8 A and practically identical to Model 4 as far as the gradient, error field and the stray field are concerned.

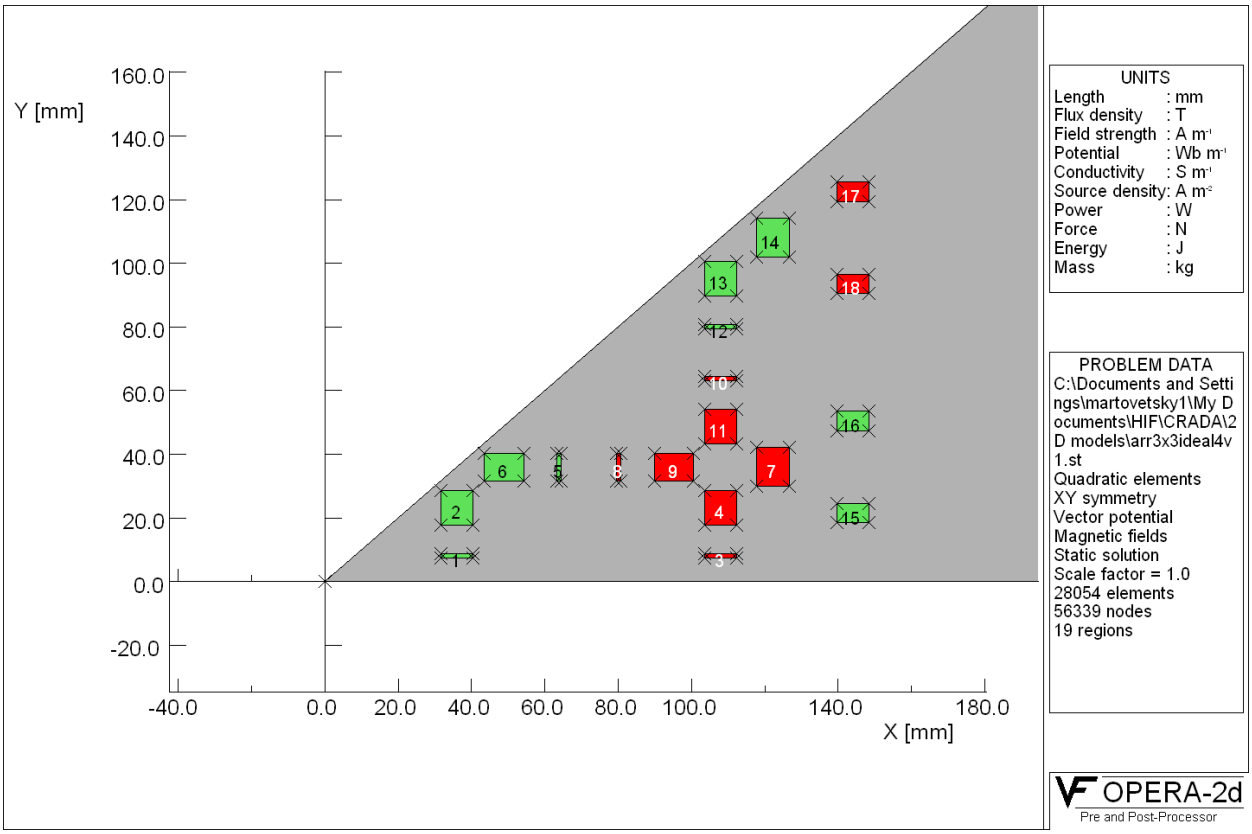

Fig. 8 A. Model 4A, a modified version of the model 4 where outmost pancakes are made as double pancakes rather than single pancake in Fig. 8. The error field and stray fields are almost identical to the model 4.

The next simplification is to merge the outer shields into continuous double pancakes without spacers. This simplification is not that critical simplification. The double pancake is needed for the inner array windings, since there is no room for the lead of the racetrack. For the shield windings, there is no room constrain and it could be done either as a single pancake (Fig.8) or as a double pancake (see Fig.8A). Nevertheless, we explore this possibility, since it eliminates at least one spacer. Fig. 9 presents this modified geometry, which we will call Model 5.

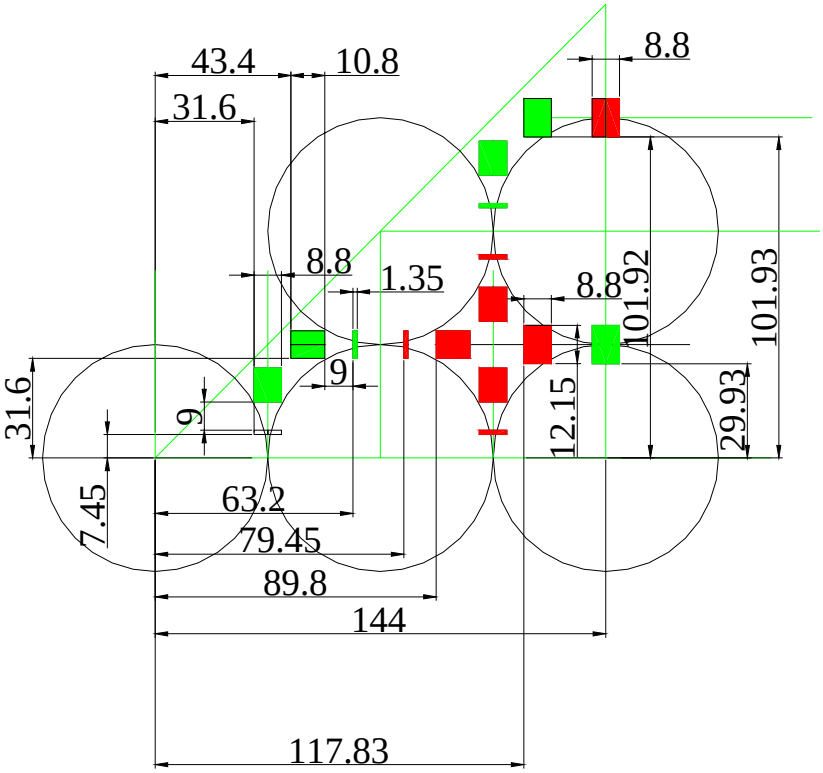

Fig. 9. Model 5 geometry.

As one can see, this Model 5 geometry is the end of our modifications of merging, since the next logical thing to do is to merge the shielding windings, which would eliminate them altogether. That would be equivalent to the elimination of all the shielding windings from the very start and we know from the previous R&D that such a geometry would not yield a high quality quadrupole field.

The next model we analyzed was a Model 6, which is different from the Model 5 by only a ferromagnetic shield, see Fig. 10.

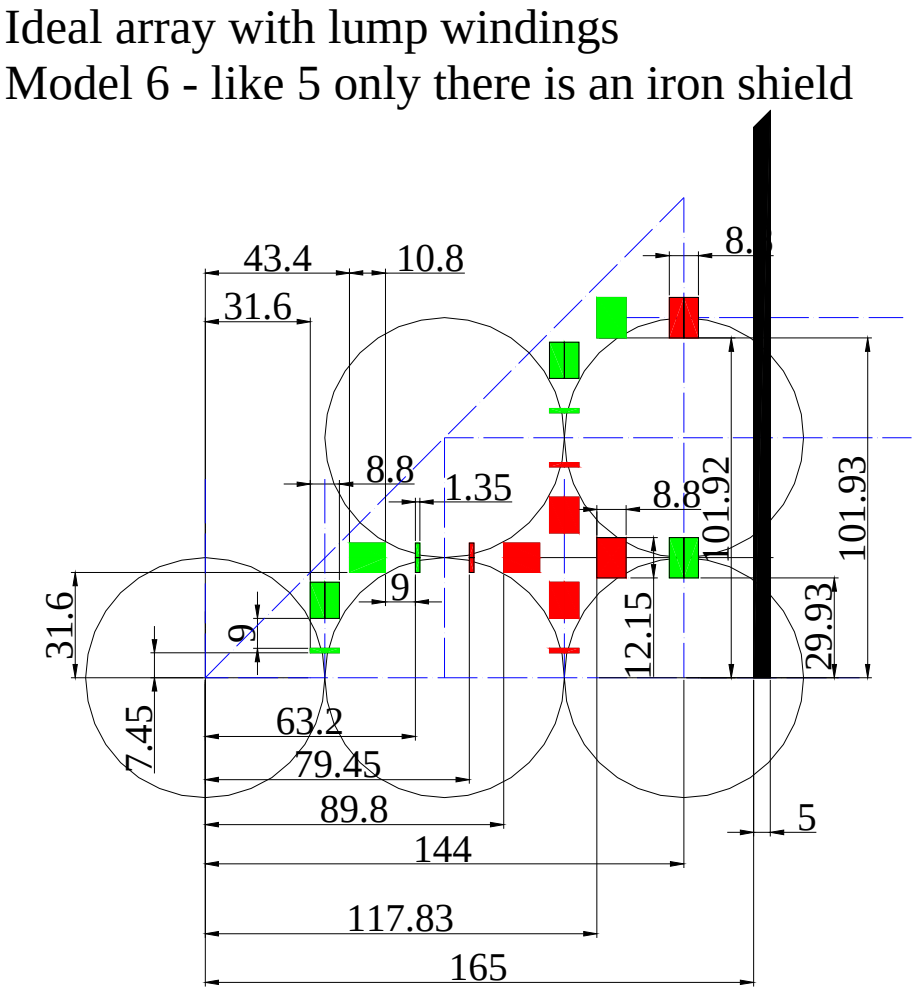

Fig. 10. Model 6.

It is time to see how our geometry modifications are reflected in the harmonics of the cells.

Gradient and error field in the studied models

Fig. 11 presents the gradients in the cells of the array.

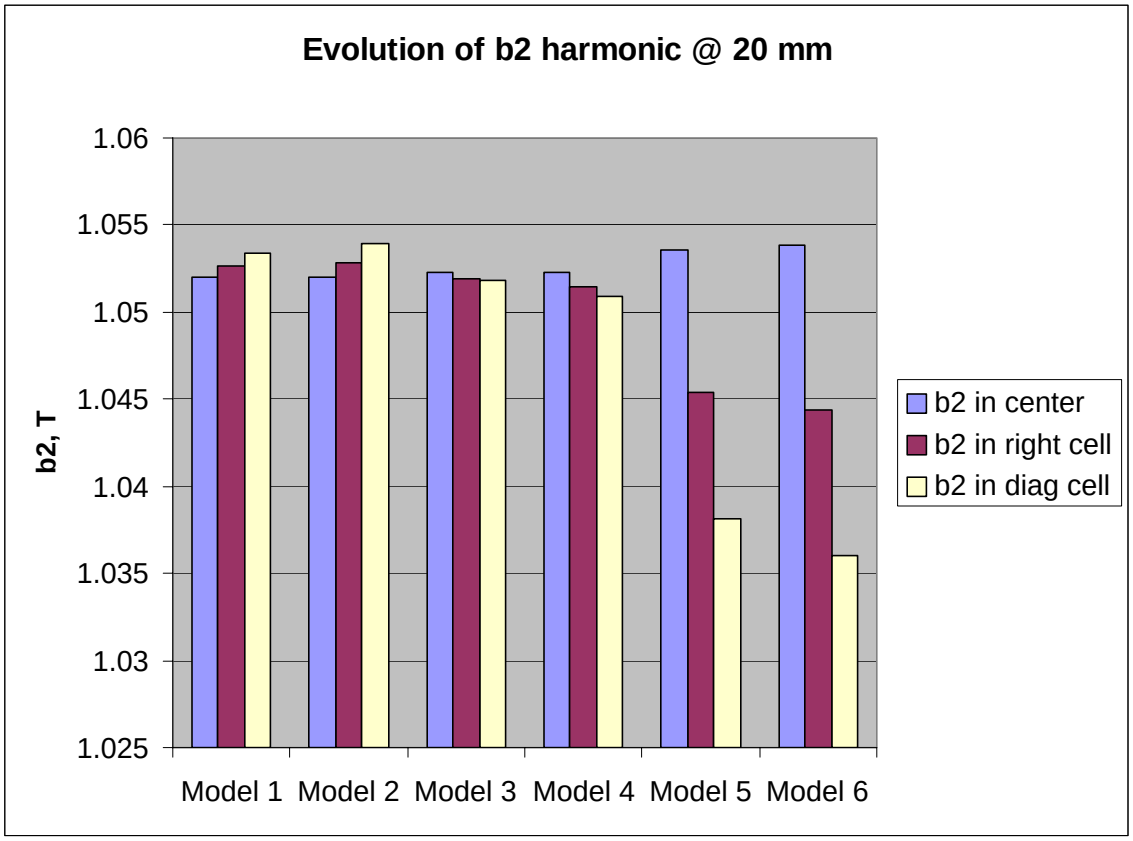

Fig. 11. b2 harmonics in the cells of eh 3x3 array versus model.

As we can see, the Models 1 through 4 give more or less uniform gradients, starting from the Model 5 the gradient in the diagonal and the right cells decreases by 1-2%.

Fig.12-14 shows the error filed in terms of normal harmonics "b_n". The integral error is calculated as:

$$Interr = sqrt(b_3^2 + b_4^2 + b_5^2 + b_6^2 + b_{10}^2) \qquad (1)$$

This integral error does not include b1 components because it is compensated separately. Other, higher harmonics are ignored because they are negligible. The a_n components (which are negligible in the center and in the right cells are not small in the diagonal cell) are not included since we select integration in the diagonal cells in such a way that they are zero and bn represent actually $c_n=sqrt(a_n^2+b_n^2)$.

The skew harmonics an (negligible everywhere except in diagonal cells) with integration around a complete circle will be shown later from the 3D analysis field. The reason for that is that in 2D models we use 45 degrees wedge geometry for analyses, so we do not integrate around the full circle in any of the cells and integration is not performed always from the horizontal axis. In the central cell we obviously integrate from 0 to 45 degrees, for the other cells – 180 degrees, 0 to 180 degrees in the right cell and –135 to 45 degrees in the diagonal one. By doing this and projecting integration to the

full circle, some harmonics will disappear, some will not. In the 3 D analysis we go full circle and we do not have to worry about symmetries.

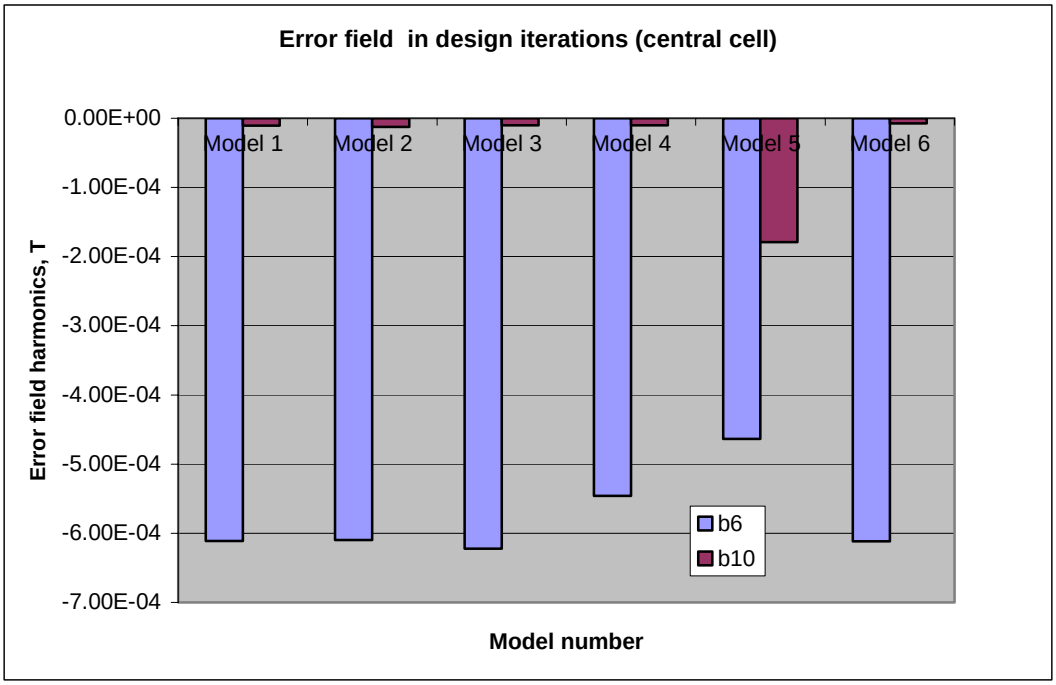

Fig. 12. Error field harmonics in the central cell

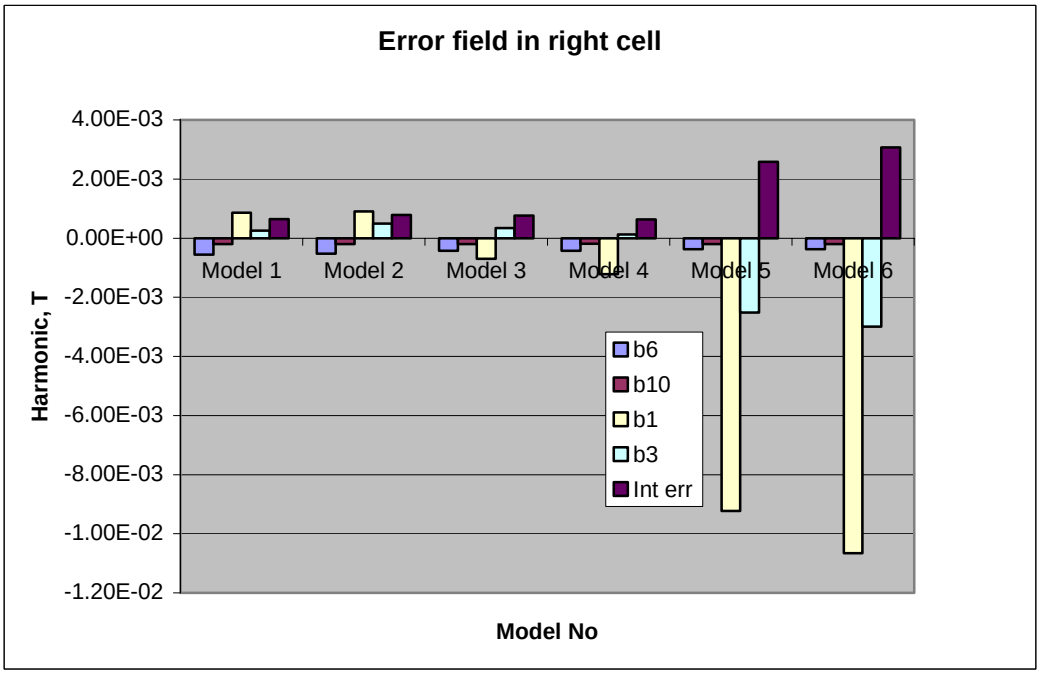

Fig. 13. Error field harmonics in the right cell

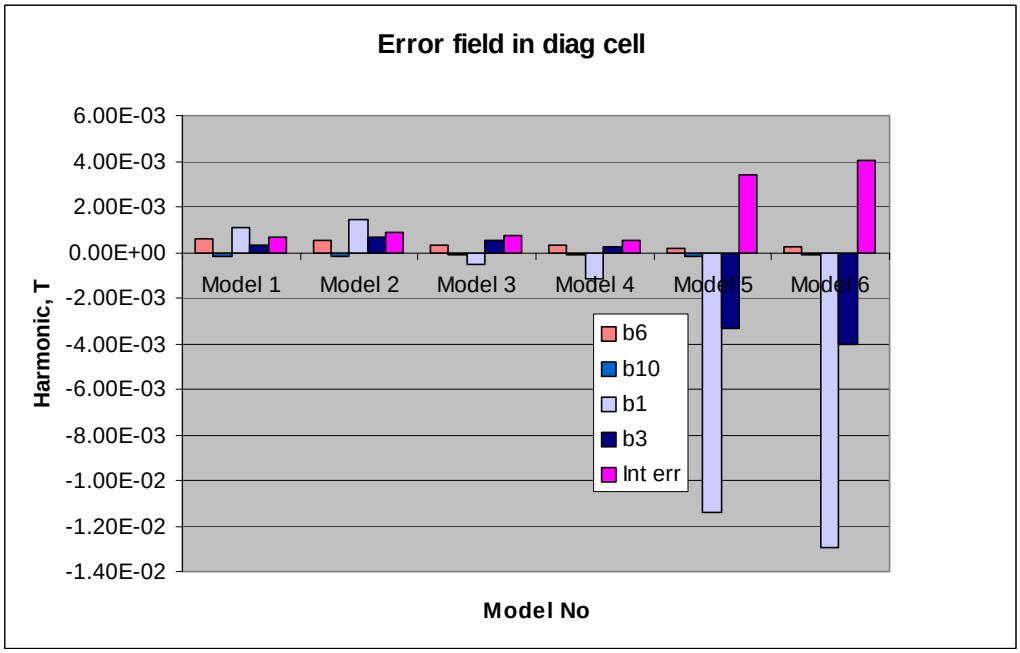

Fig. 14. Error field harmonics in the diagonal cell

Fig. 11-14 shows the gradient and the error field components in the models 1-6. Looking at the error evolution with the changes in the model, one can immediately see that the change made in the Model 5 is the most damaging one. Also, there is some noticeable difference between Models 5 and 6, which shows that if the iron shield is close enough, it may influence the field quality in the cells. The effect is not necessarily good, but if optimized, we believe that the iron shield may be a positive factor for the cells quality, however, this issue is outside of the scope of this study.

Let us take a closer look at the dipole harmonic, shown in Fig. 15. Although its amplitude is the largest, it goes to zero with the shift of the beam line by 0.2 mm, which is less than expected accuracy of the beam alignment (0.5 mm). In addition, this dipole component could be easily compensated by the correction coils. The next largest error component is the 6 – pole harmonic b3. That component is not that sensitive to the center of the beam and needs to be compensated by adjustments in the main windings.

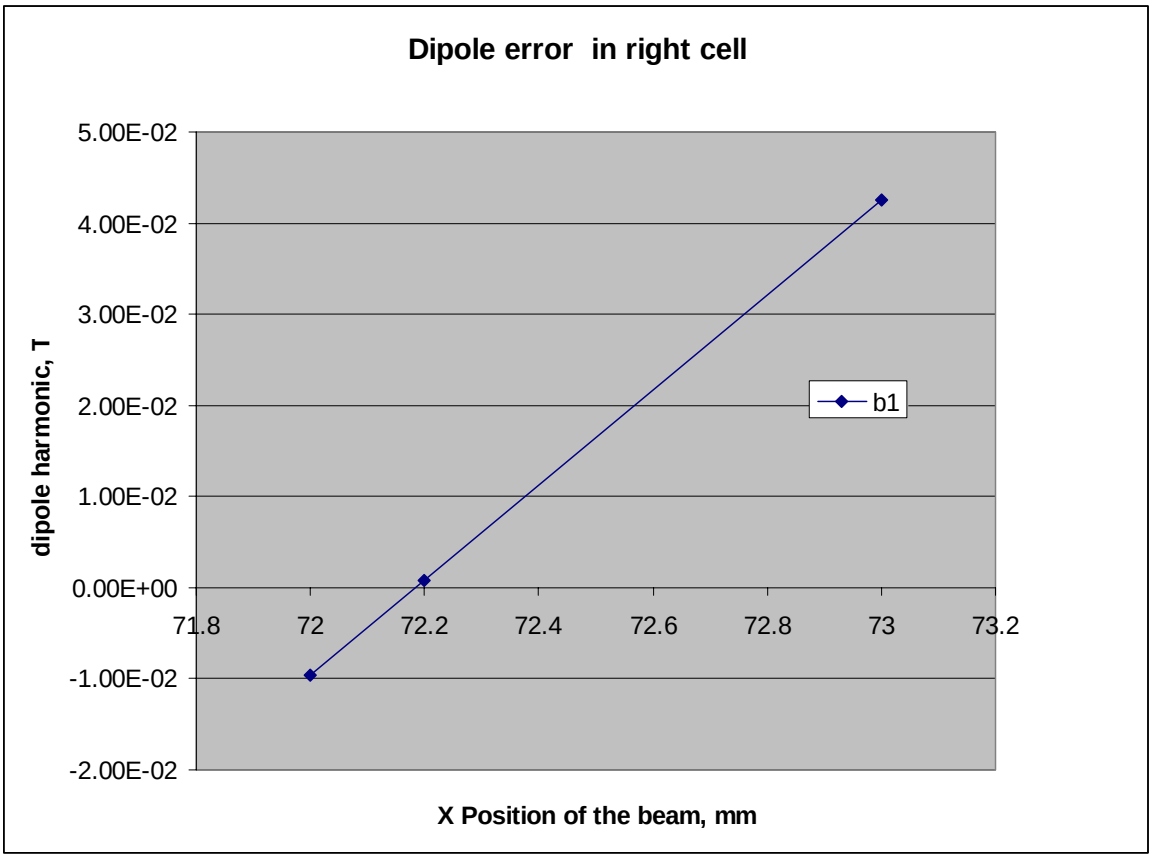

Fig. 15. Dipole field amplitude versus position of the beam center.

Shielding the stray fields in 2 D model

We studied several cases of shielding. Fig. 16 shows the stray field (10 G increments, line 2 corresponds to 10 G) for the Model 4 (no shield).

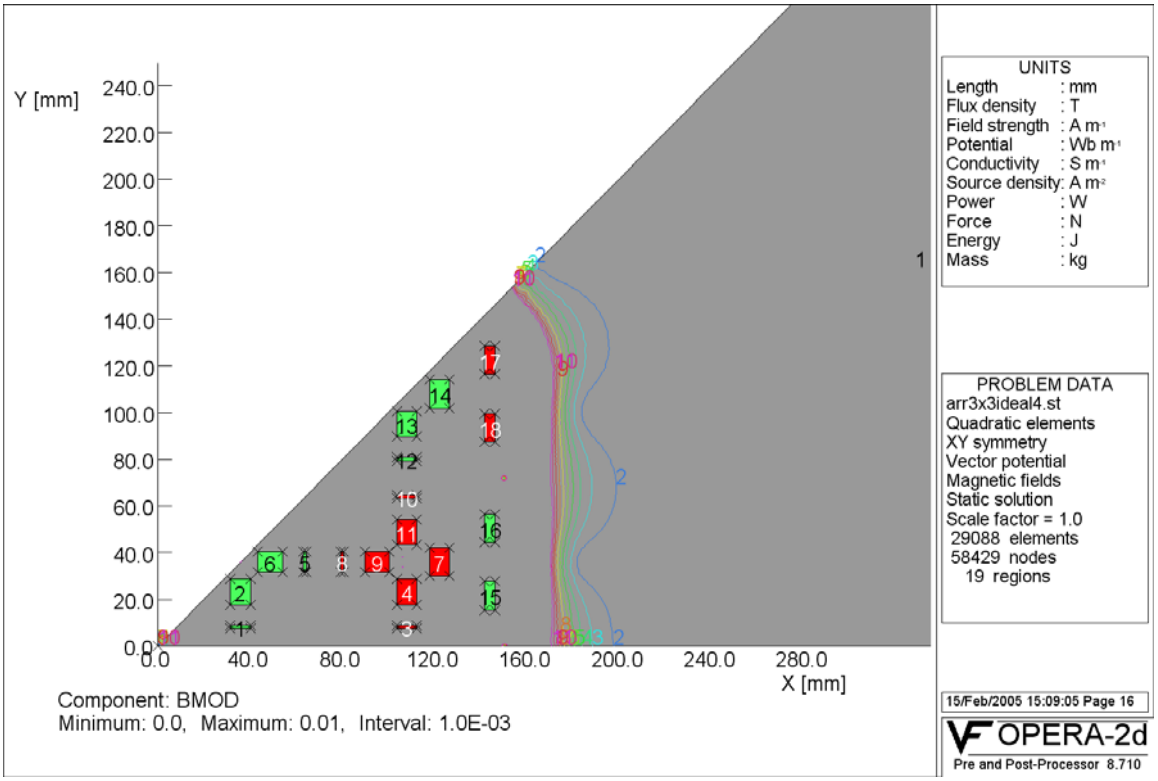

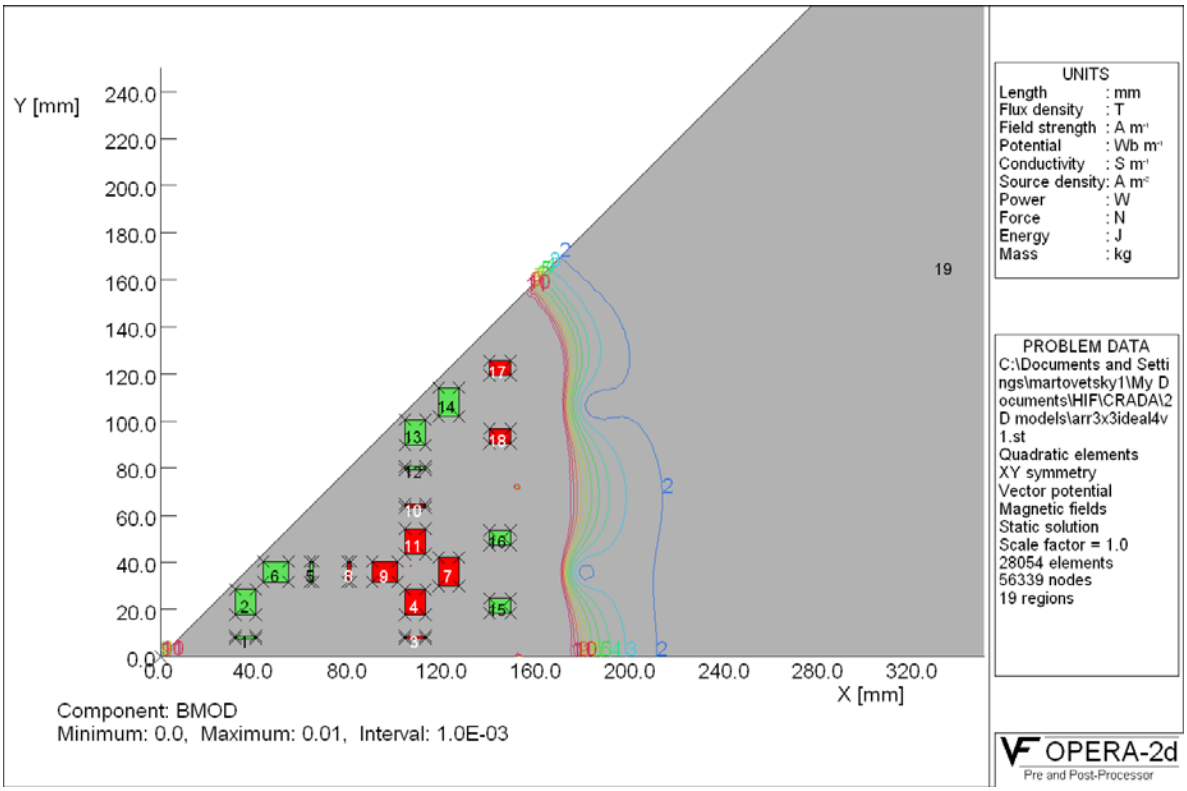

Fig. 16. Stray fields in the Model 4 and 4 A.

These results indicate that the stray field will not propagate outside of the cylindrical cryostat and possibly will not require any shielding in the radial direction.

Fig. 17 shows the stray fields for the Model 5.

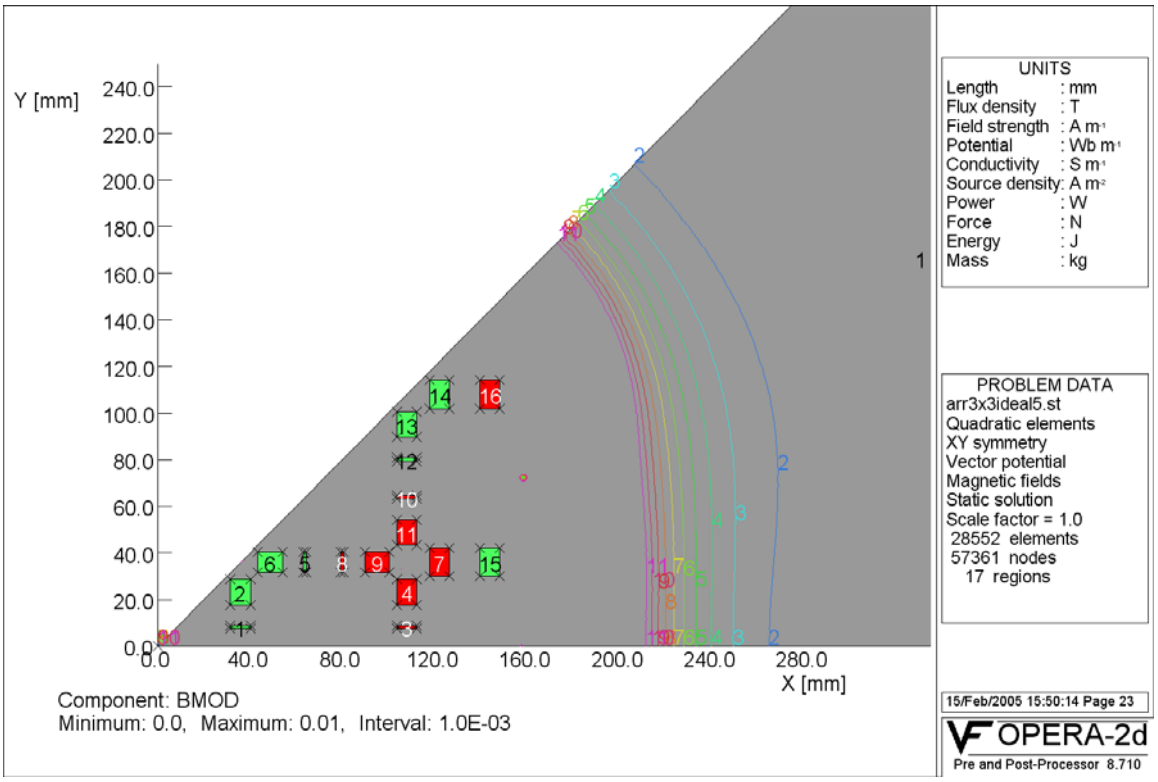

Fig. 17. Stray fields in model 5.

The stray field propagates significantly farther in the model 5 than in the model 4 and this shows that the changes from model 4 to 5 result in significant increase of the stray field along with the error field.

Model 6, illustrates how efficient is the 5 mm thick iron shield. Fig. 18 shows that the stray field in the Model 6 is completely contained inside the shield (note that the field lines are all in the corner).

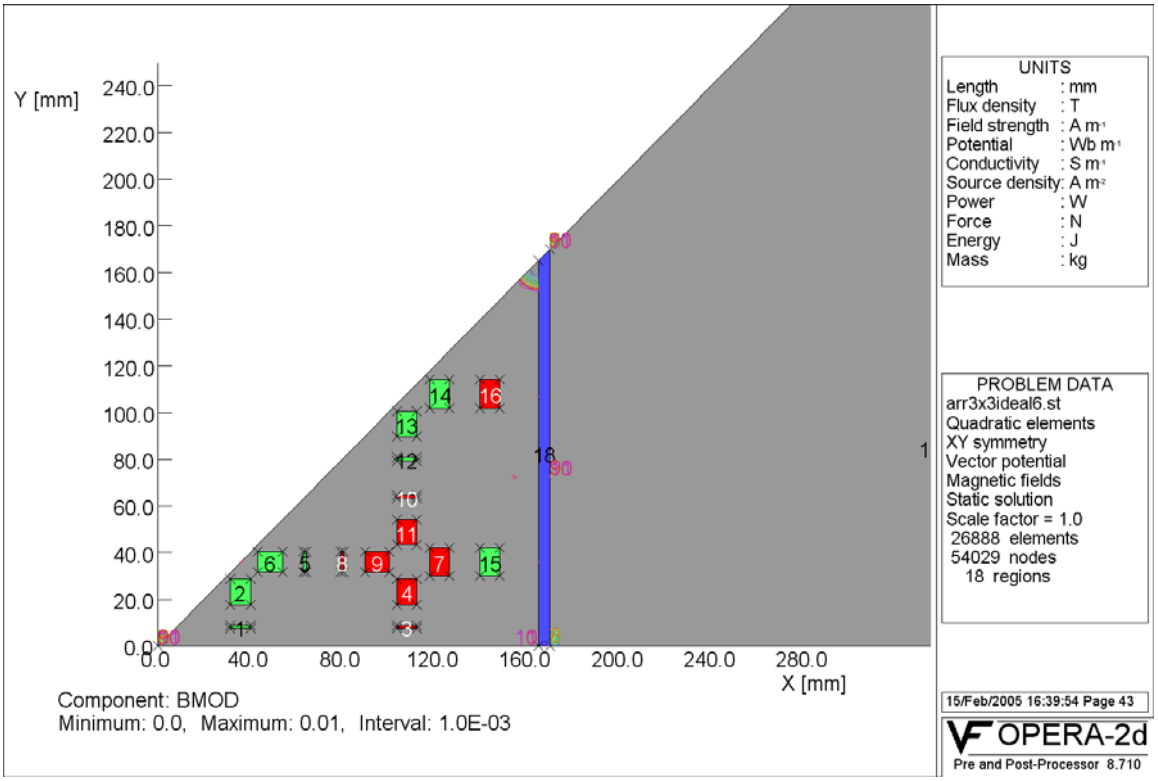

Fig. 18. Stray fields (10-100 G) are completely contained inside the shield.

Assuming that the final array will be contained in a cylinder, it is reasonable to check if 3 mm steel shield at a radius of 240 mm will be sufficient to shield the field. This dimension assumes that it will be the vacuum vessel wall of the array, similar to the low carbon steel vacuum wall in the accelerator magnets. Fig. 19 shows that such a shield would be quite effective to practically eliminate the stray field.

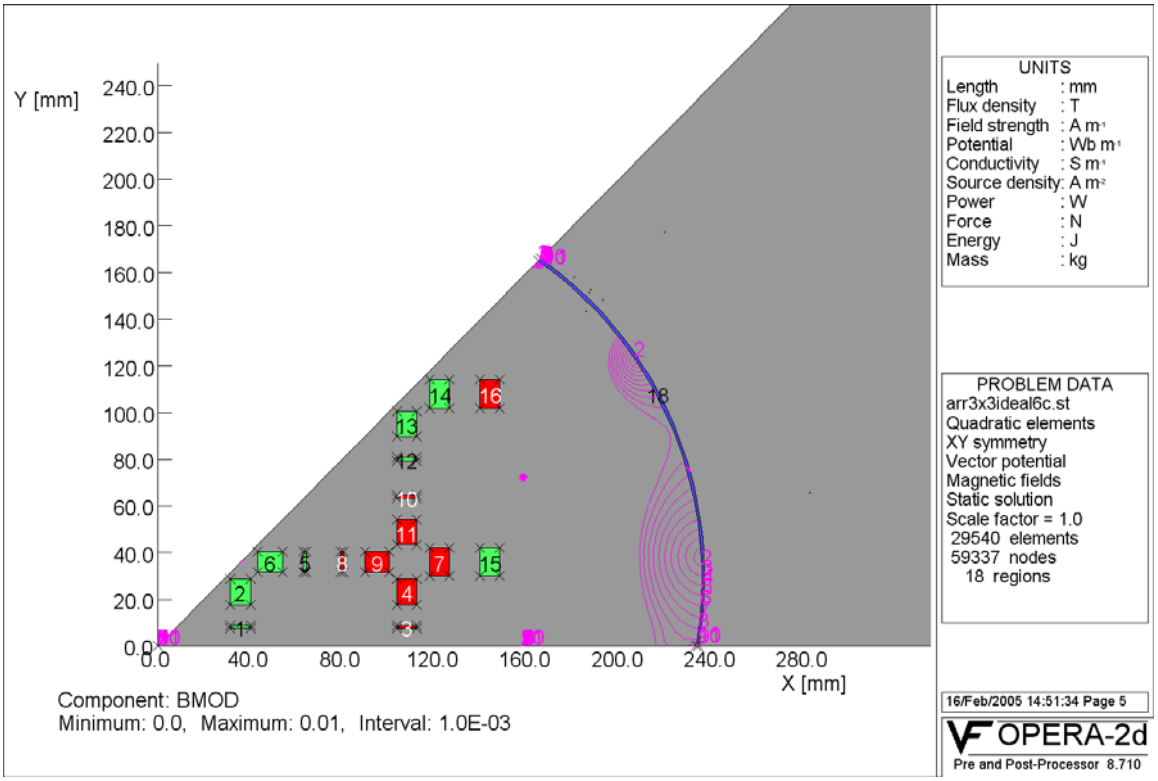

Fig. 19. Stray field in the Model 5 with a cylindrical iron shield 3 mm thick.

Optimization of the Model 5

It is quite clear from Fig. 11-14 that the principles used in design of the 3x3 array are applicable to an arbitrary size rectangular array, like 5x5, 10x10, 6x8, etc. Model 4 is a clear limit in simplifications at given requirements for the magnetic field. The Models 5 and 6 require improvement.

Our next activity is to see if we can improve Model 5 by shifting winding packs 7 and 14. The reason why we constrain ourselves to only these winding packs is as follows. In principle, there should be a solution (at least theoretical) for good field inside the right and diagonal cells and low field outside if we make all space in the array available for windings. On the other hand, that would clearly be a step back in the simplicity in comparison with the Models 4 or 5. Therefore, we consider a promising option only if it does not complicate the geometry and increase the cost too much. We also do not want to touch the windings from the "infinite array" since that means another kind of windings should be introduced to add to complexity and eventually, the cost of the magnets. Our approach obviously does not cover all possibilities, but seems reasonable to explore.

The problems with the error field clearly came from the merging the outmost shielding windings in the step from the Model 4 to the Model 5 and we can always go back to the Model 4 or 4A. However, we will look for a solution based on the Model 5 when the outmost windings are merged. Looking for a lower error field, we will move winding packs 7 and 14 in the Model 5 (see Fig.17). Winding pack 14 has a limit on how far it can go up due to interference with the other cell. Obviously,

there is a limitation in how close the winding pack could be to the apertures due to interferences with the other windings. Since many harmonics contribute to the error field we will use the integral error defined above in the relationship (1).

Fig. 20 shows effect of moving winding pack 14. We see that the error field is not sensitive to the position of the winding pack 14. This statement is true also for moving winding pack 14 along the x-axis.

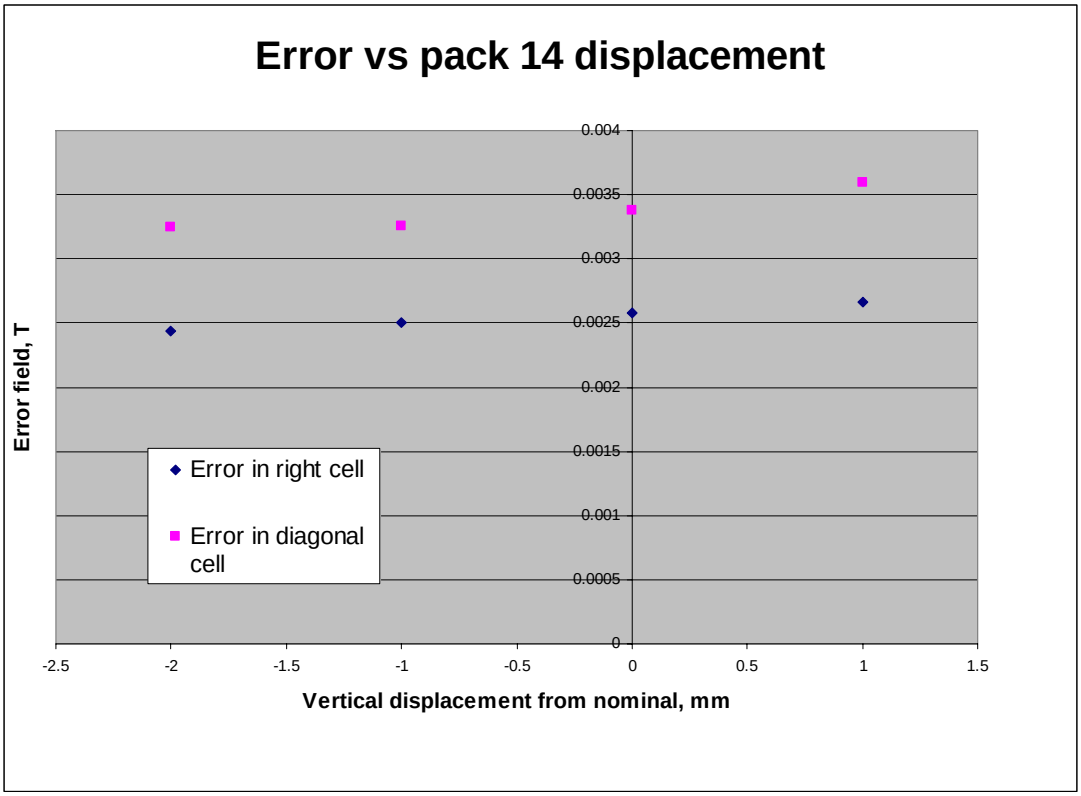

Fig. 20. Effect of the winding pack 14 (see Fig. 17 for definitions).

Fig. 21 shows the error field change as the winding pack 7 is moved around its position up and down.

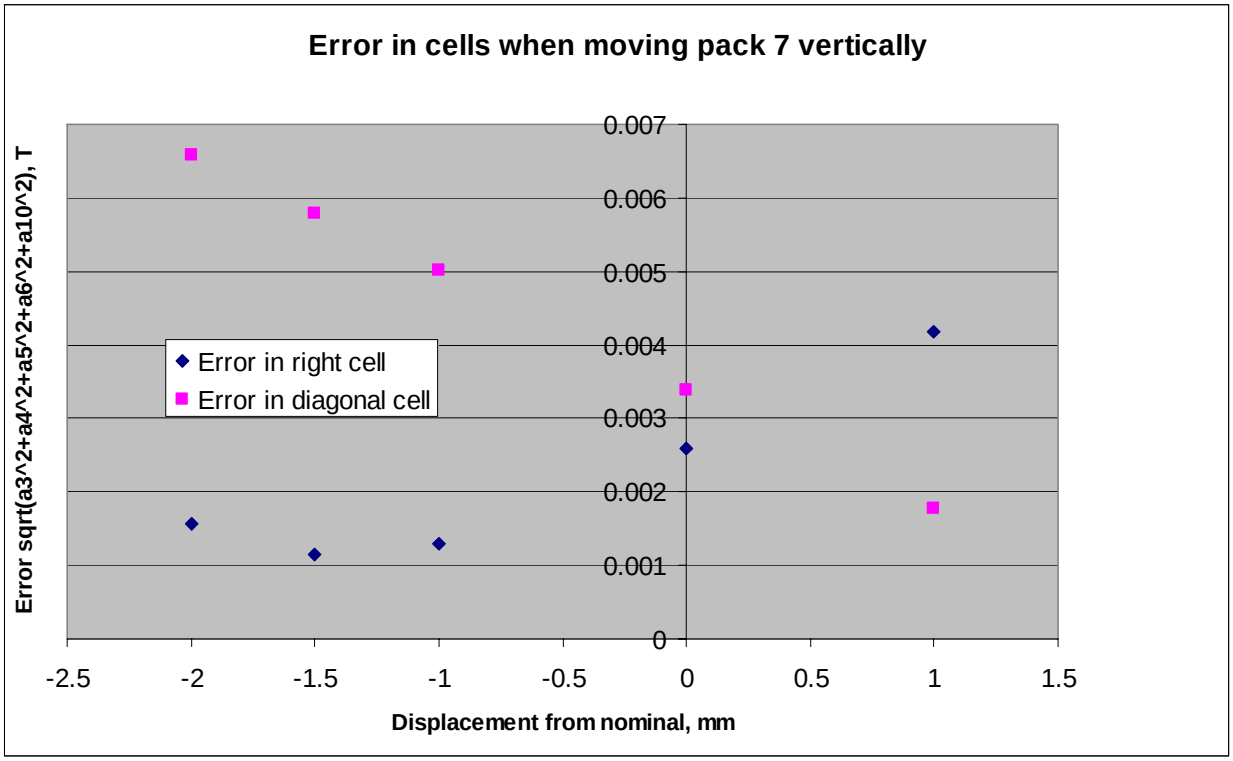

Fig. 21. Effect of the winding pack 7 (Fig.16) on the error field.

Note, that positioning of winding pack 7 helps improve the error, but in the reasonable range the integral error is never better than 1e-3. Also, when the field in the right cell improves, the field in the diagonal cell becomes worse. That suggests that splitting winding pack 7 might be able to improve the field quality. We also checked error field change versus positioning winding pack 7 along the x-axis and found that it was not effective.

Fig. 22 shows the idea of splitting winding pack 7 into two. Since it is a model from the Opera 2D code, it automatically re-numbered the conductors area and what was the winding pack 7 in Fig. 17 became winding packs 17 and 18.

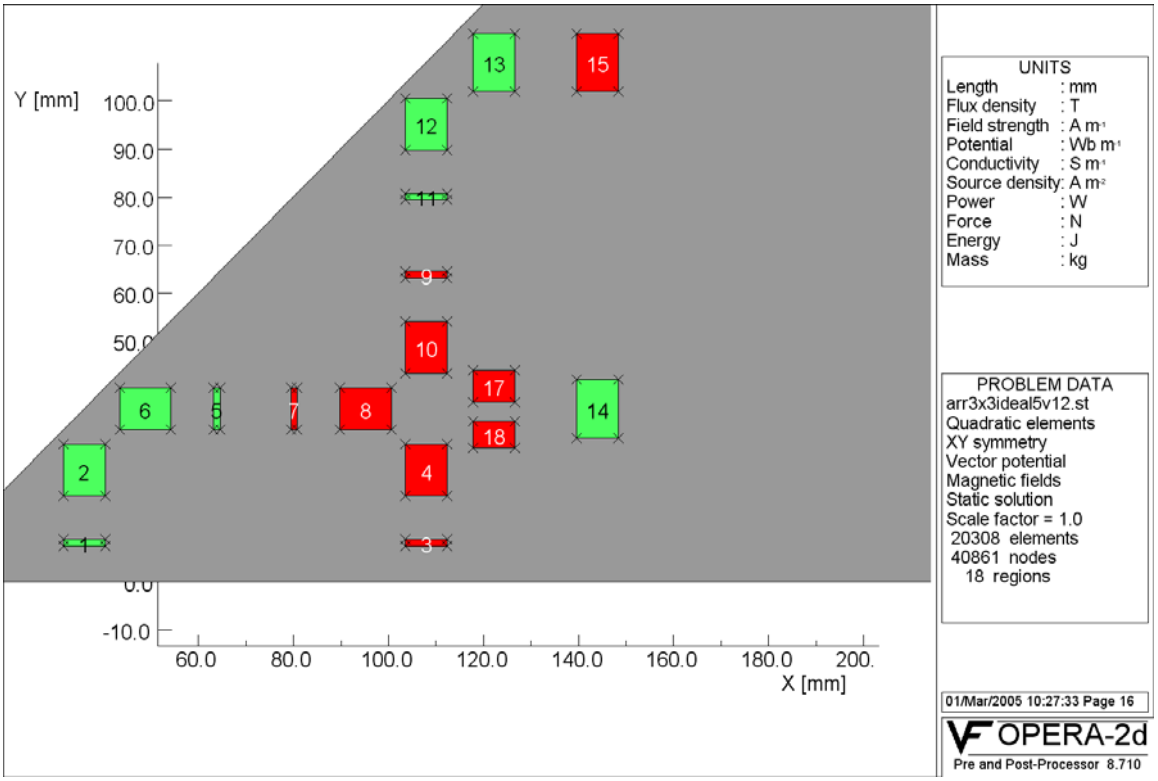

Fig. 22. Opera 2D model with the split winding pack

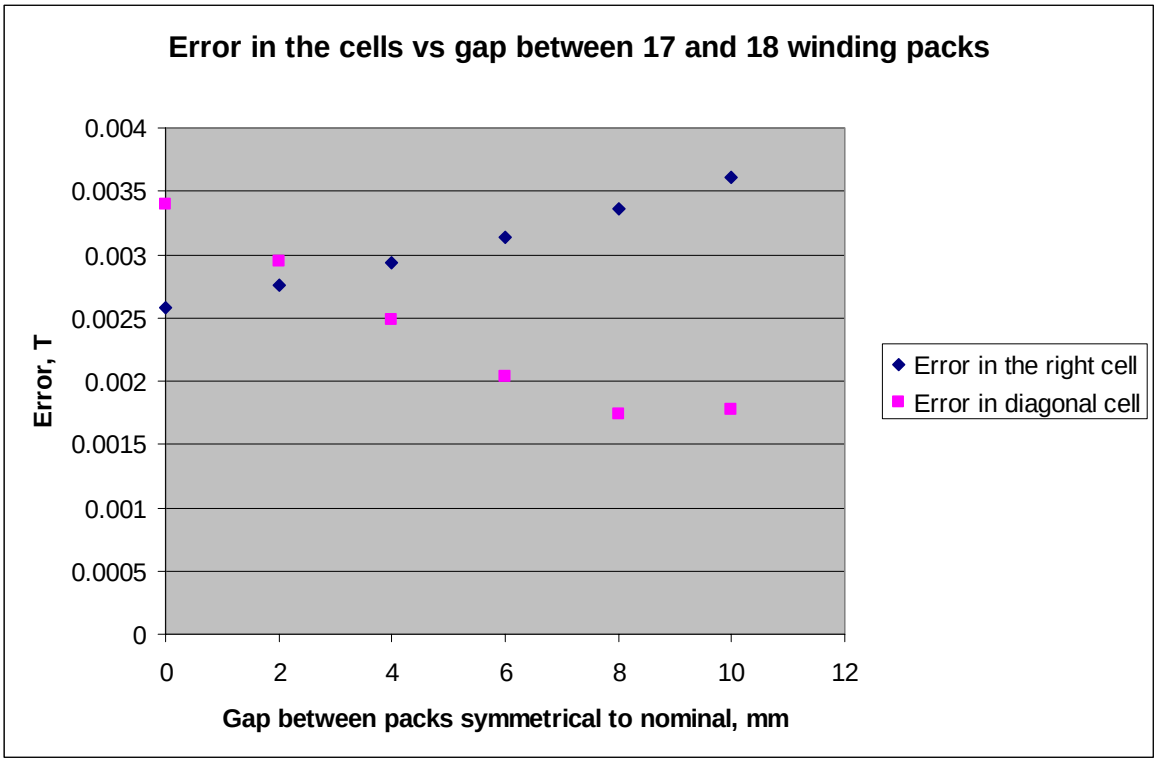

Fig. 23. Effect of the gap on the error field in the array

Fig. 23 shows effect of the gap on the error field. As we can see, the gap does not reduce the error field very much. A possible explanation to that is that the position of winding packs 7 and 14 in Fig. 17 are close to the optimal and moving them around will not reduce error fields.

Although this study does not draw any strict conclusions about possibilities of reaching a better field by manipulating the shielding winding packs 7 and 14, we could not find any indication that it exist within practical range of windings.

This attempt at improving Model 5 suggests that Model 4 (or 4A) is the best practical configuration for an array (single or double pancakes of the outmost shielding winding pack are both acceptable). We see also that Model 5 has about 10 % higher peak field than Model 4, which means lower gradient by about 5% than Model 4.

Since we were unable to obtain significant improvement in simplicity and error field in our optimization effort of Model 5, within the scope of work we stop our effort in looking for a better 2D geometry and will proceed with the 3 D model studies based on the model 4. Before we do that, however, we would like to see how much of a gradient we could obtain with the cable we assume in the design.

Maximum achievable gradient

Fig. 24 shows the load line for the peak magnetic field and the critical currents for the Rutherford cables used in the previous prototypes in the previous R&D effort on focusing magnets. As we can see if we use a Rutherford cable made out of SSC inner strands, redrawn down to 0.648 mm diameter, we can reach 5T peak field at 5 kA and 85 T/m gradient. The cable made out of outer strands would have about 10% lower gradient. As operating current is defined as 70% of the short sample current, the operating gradient will have about 60 T/m for the cable with the SSC inner strands. Thus the specifications for the gradient could be met with the inner SSC strand cable, but not with the outer SSC strand. The current density in copper is also close to the specified 1500 A/mm^2, thus, the cable made of the SSC inner strand is barely adequate to meet the specs.

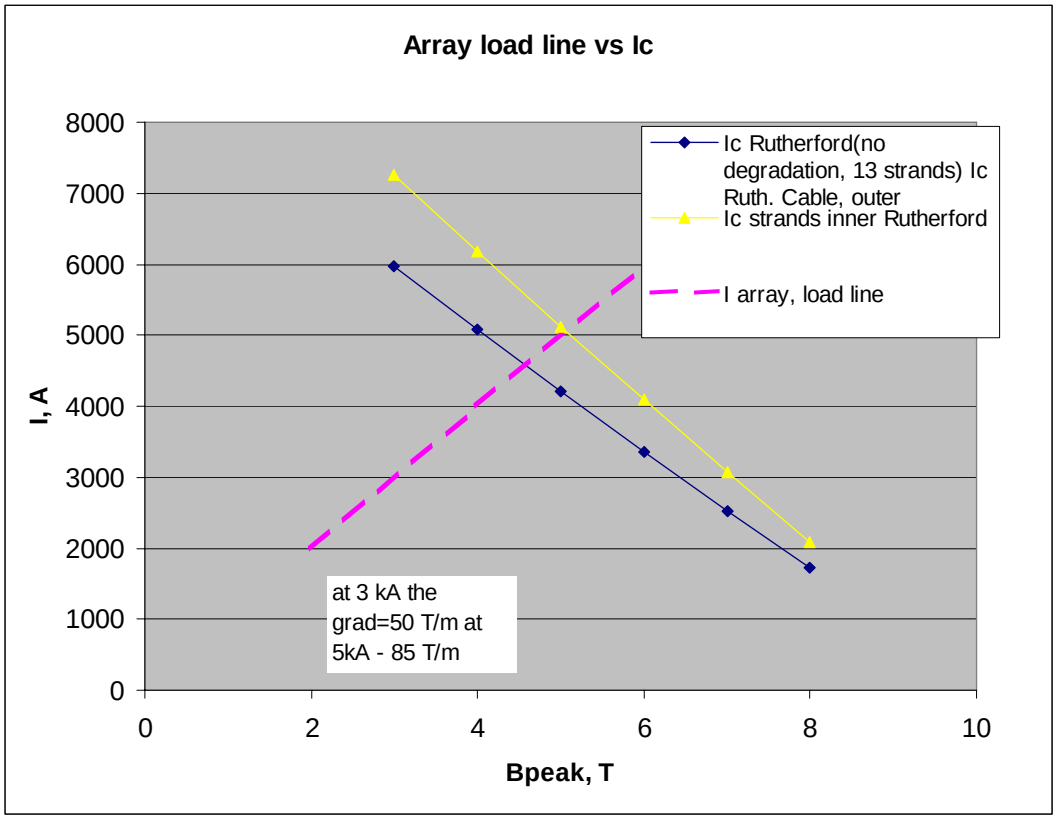

Fig. 24. On the maximum achievable gradient in the 3x3x array.

3D studies of the 3x3 array based on Model 4

We built the 3D model based on the 2D Model 4. The ends of the racetracks have minimum radius of curvature of 8 mm (except few one-turn pancakes, which are located at 7.45 mm from the symmetry plane, so the radius of curvature at the ends is 7.45 mm for those turns). The length of the pancakes is 600 mm. All the internal pancakes have the spacer in the ends the same as in the median plane.

Fig. 25 shows the geometry of these windings, one half of them, since they are symmetrical relative to the median plane. There are three types of the pancakes. We call them array pancakes, outmost shield windings and inner shield windings. At this point we do not introduce any ferromagnetic shields.

Array windings

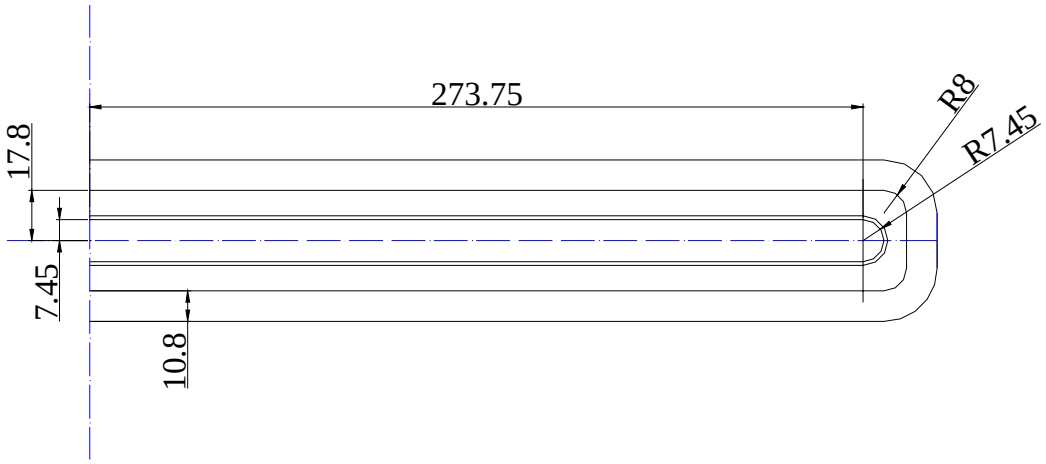

Inner shielding racetrack

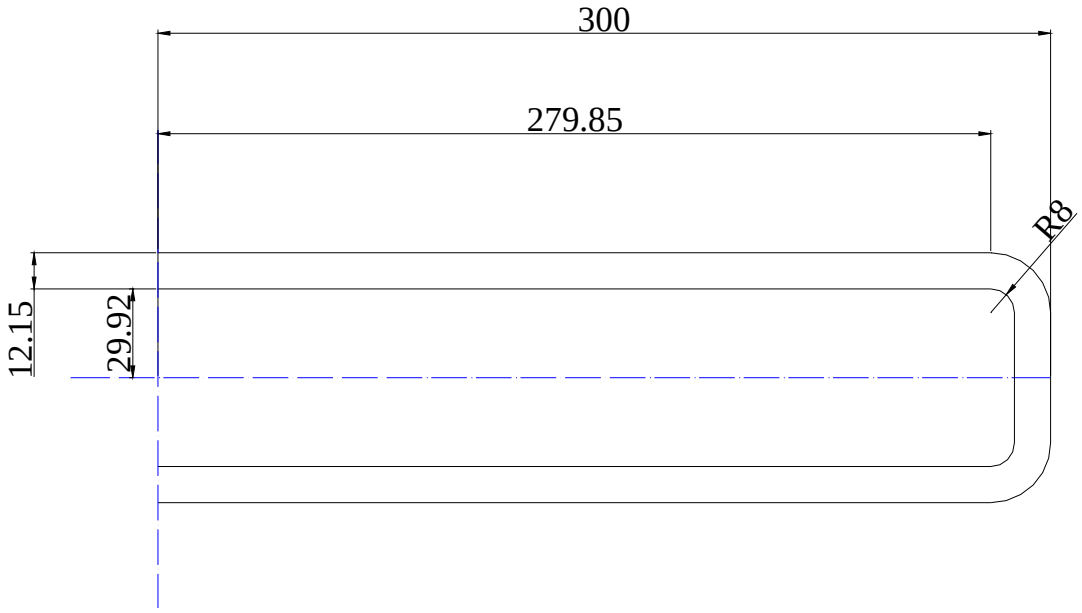

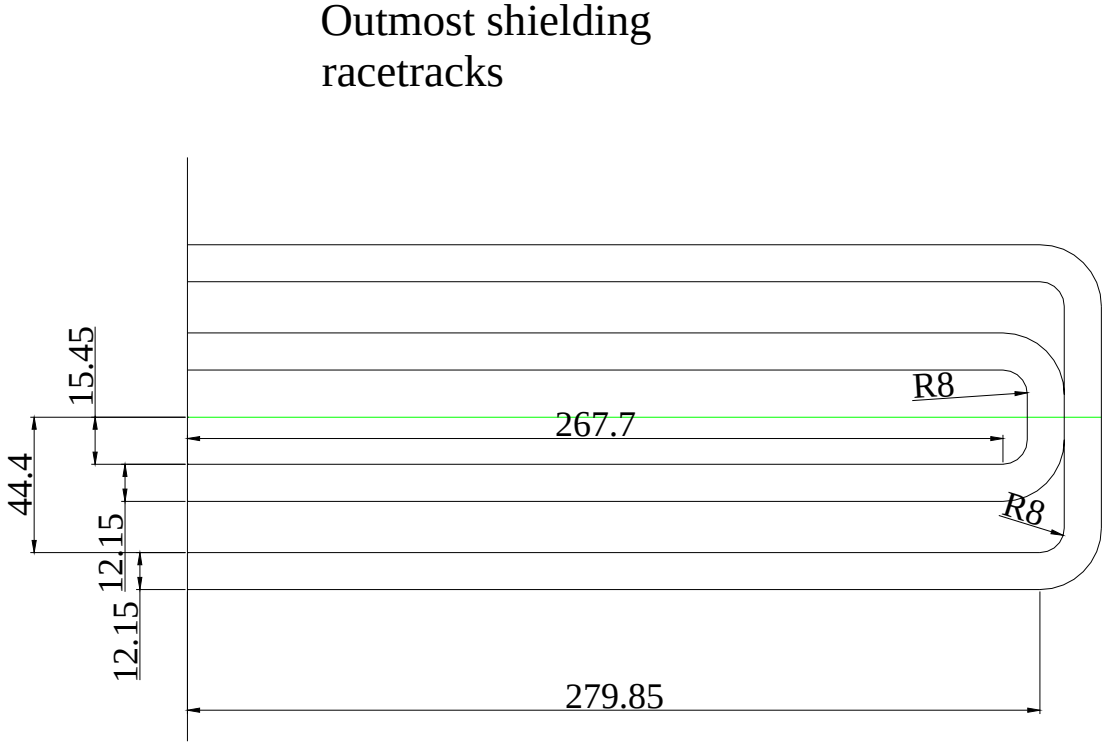

Fig. 25. Geometry of the racetracks for 3D studies for Model 4.

The shielding windings have no spacers in the ends, since it is not expected that the peak field will be an issue there.

Fig. 26 shows the coils of the 3x3 array on the basis of Model 4.

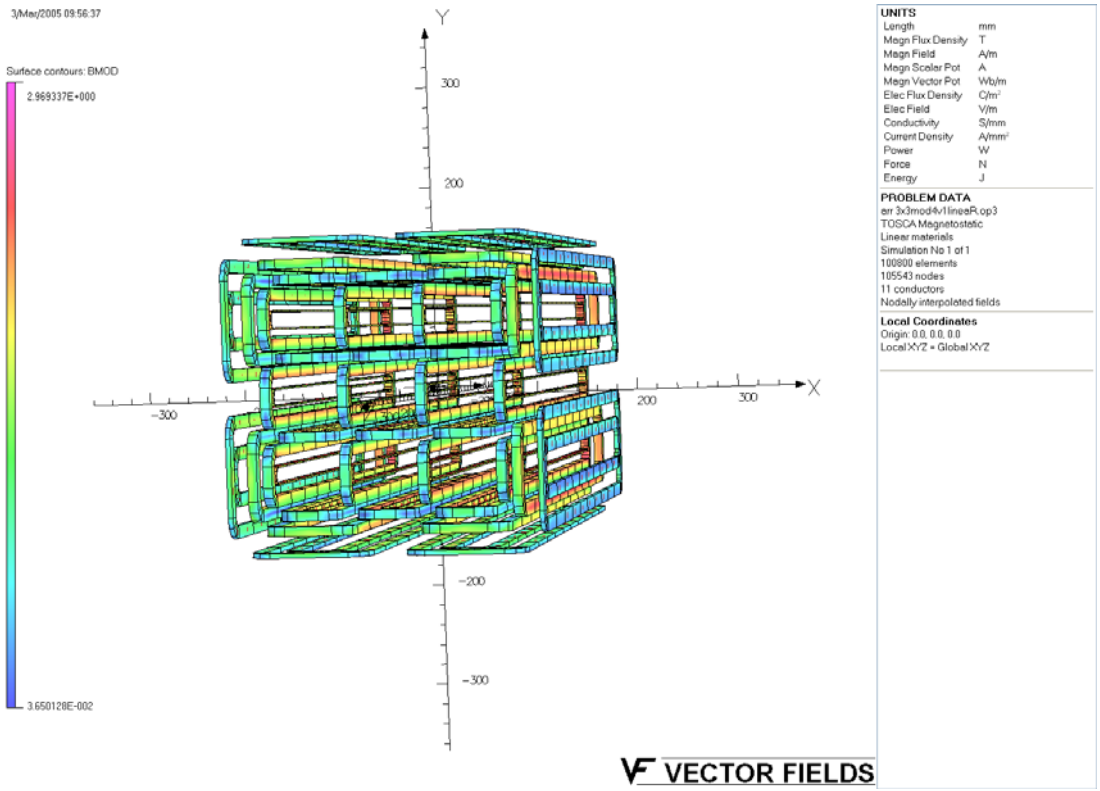

Fig. 26. 3x3 array windings based on the 2D Model 4. The color indicates the magnetic flux density B.

The peak field in the coils is 2.96 T at 500 A/mm^2 in the winding pack. The 3D field is about 6% higher than in the 2D model, which indicates that the ends do not create too high field concentration and do not require further optimization. The most loaded pancake (see Fig. 27) is the pancake surrounding the diagonal cells from outside (winding packs 11 and 13 in Fig. 17.)

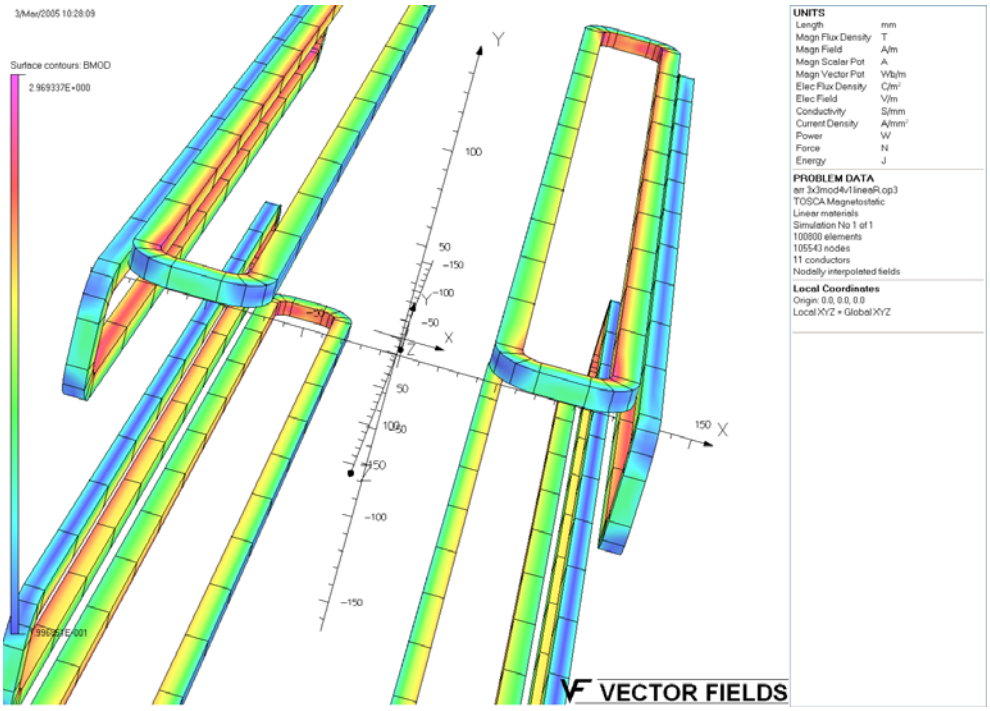

Fig. 27. Peak field in the mostly loaded pancake.

We computed gradient and Fourier harmonics at 20 mm radius in all the cells of the array along the axis of the cells. The gradient in the cells is shown in Fig. 28.

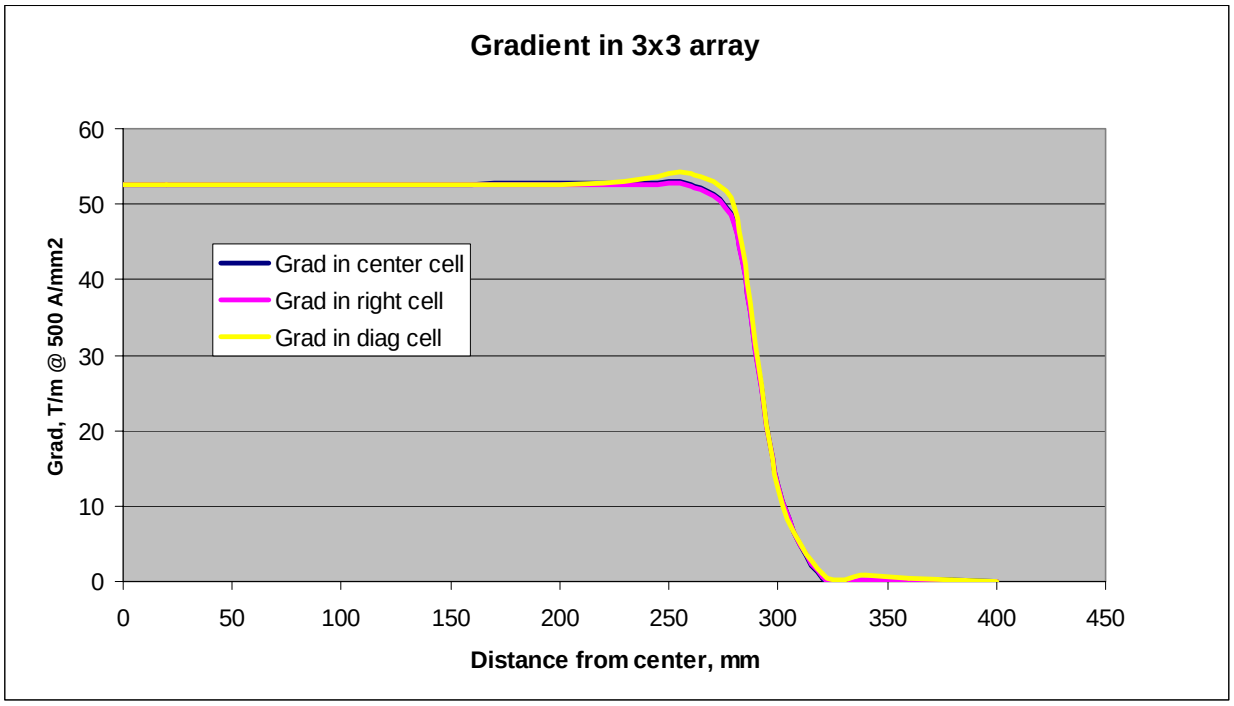

Fig. 28. Gradient in the array cells.

As one can see, the gradient in the diagonal cells is slightly higher (1%) than in the other cells.

The error field in the cells is shown in Fig. 29-31.

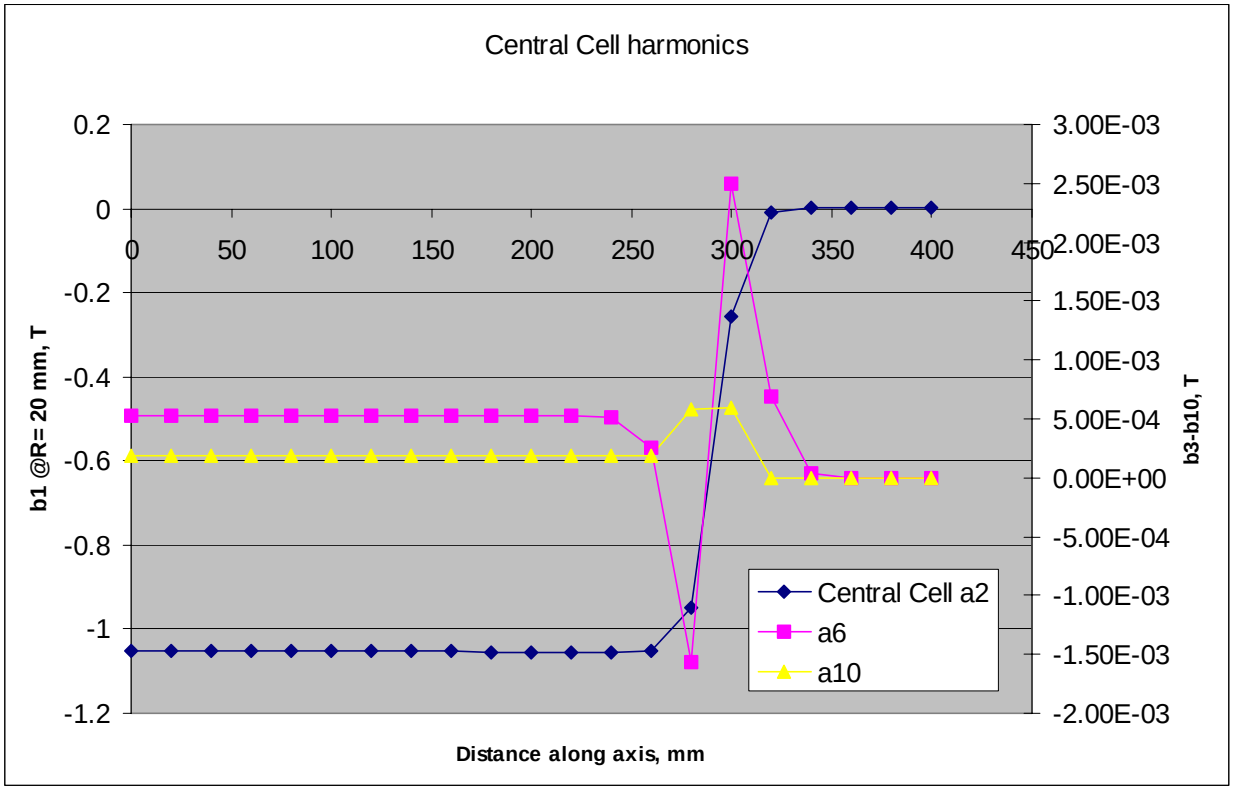

Fig. 29. Error field harmonics in the central cell of the array

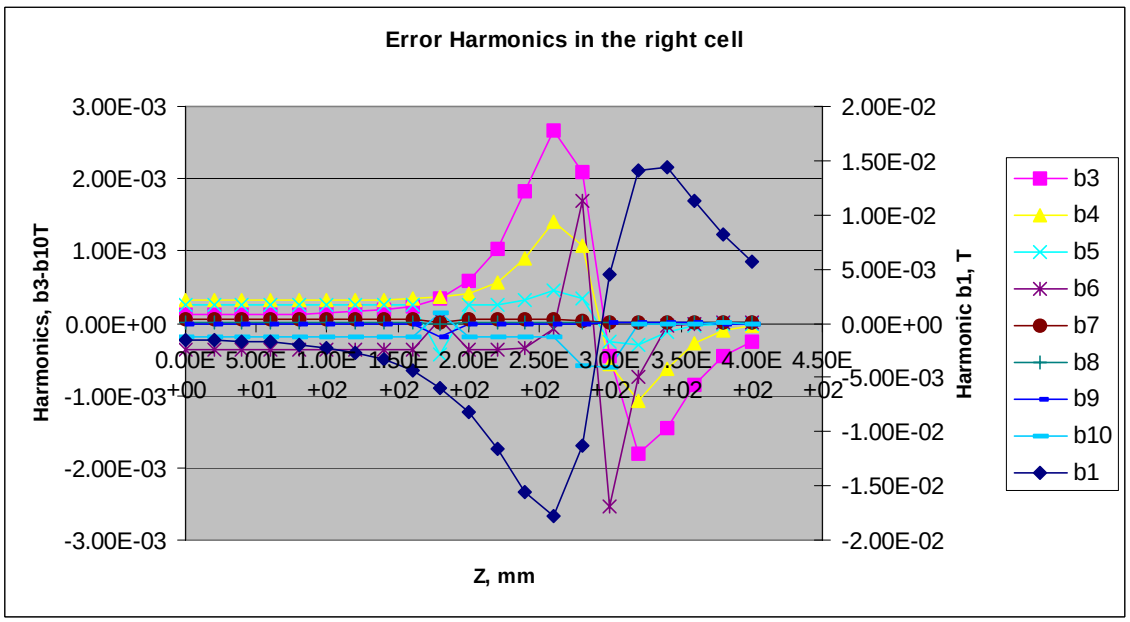

Fig. 30. Error field harmonics in the right cell of the array

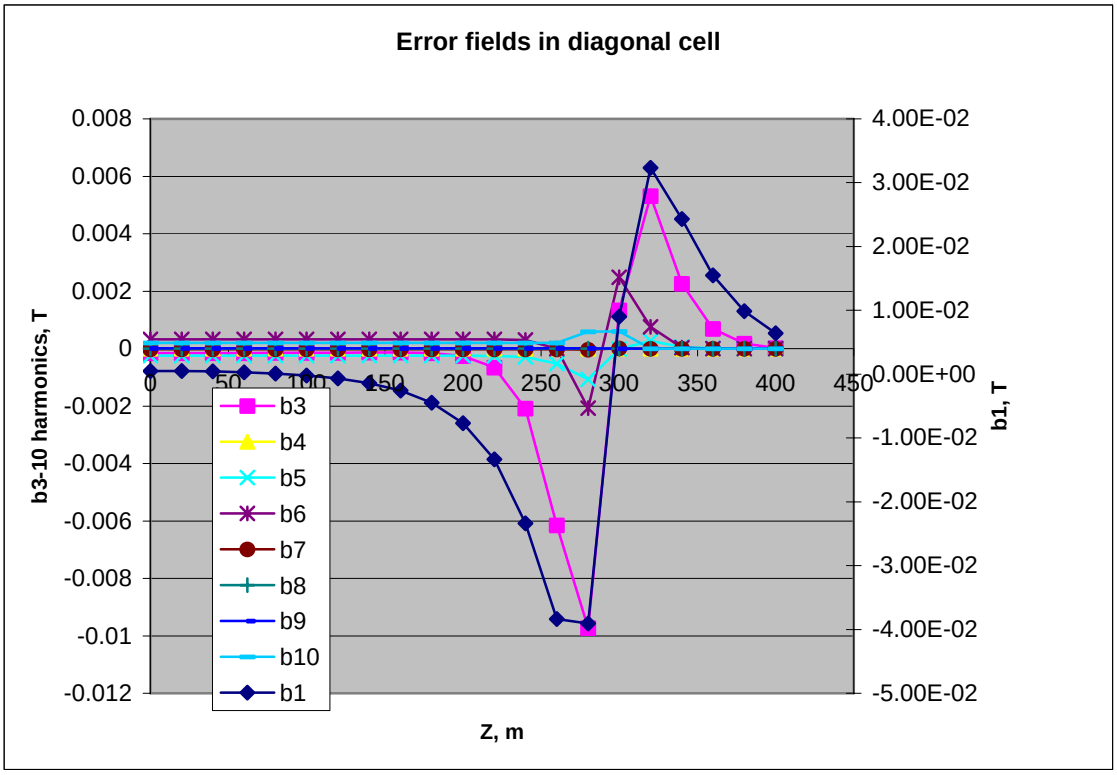

Fig. 31. Error field harmonics in the diagonal cell

As one can see, the field quality in the central cell is significantly better than that in the other cells because of the symmetry and remote location from the boundaries. The contribution to the error field in the right and the diagonal cells mostly comes from the a1 and a3 harmonics. We already discussed that the dipole component will be compensated independently, but the b3 harmonics need to be small by design. For the worst cell, the diagonal cell, integration along the length gives an average b3 component of 7e-4 T, which is within the specifications.

Thus the 3D analysis confirms that it is possible to find a configuration with the racetrack windings with high quality magnetic field in the focusing array.

Skew harmonics in the cells

The skew components of the error field are zero in the central cell and in the right cell due to the symmetry. In the diagonal cell it is not so. Table 2 gives the normal and skew harmonics in Tesla versus length (z in mm) in the diagonal cell at 20 mm in T.

Table 2. Normal and skew harmonics in the diagonal cell in 3D for Model 4.

z	b1	b2	b3	b4	b5	b6	b7	b8	b9	b10
0.00E+00	5.00E-04	-1.05E+00	-1.54E-04	-5.57E-09	-2.49E-04	3.19E-04	-2.77E-05	-1.24E-09	5.88E-06	1.99E-04
2.00E+01	4.80E-04	-1.05E+00	-1.54E-04	-5.57E-09	-2.49E-04	3.19E-04	-2.77E-05	-1.24E-09	5.88E-06	1.99E-04
4.00E+01	4.16E-04	-1.05E+00	-1.53E-04	-5.57E-09	-2.49E-04	3.19E-04	-2.77E-05	-1.24E-09	5.88E-06	1.99E-04
6.00E+01	2.96E-04	-1.05E+00	-1.52E-04	-5.57E-09	-2.49E-04	3.19E-04	-2.77E-05	-1.24E-09	5.88E-06	1.99E-04
8.00E+01	1.03E-04	-1.05E+00	-1.49E-04	-5.57E-09	-2.49E-04	3.19E-04	-2.77E-05	-1.24E-09	5.88E-06	1.99E-04
1.00E+02	-2.01E-04	-1.05E+00	-1.46E-04	-5.57E-09	-2.49E-04	3.19E-04	-2.77E-05	-1.24E-09	5.88E-06	1.99E-04
1.20E+02	-6.71E-04	-1.05E+00	-1.42E-04	-5.57E-09	-2.49E-04	3.19E-04	-2.77E-05	-1.24E-09	5.88E-06	1.99E-04
1.40E+02	-1.40E-03	-1.05E+00	-1.37E-04	-5.57E-09	-2.49E-04	3.19E-04	-2.77E-05	-1.24E-09	5.88E-06	1.99E-04
1.60E+02	-2.57E-03	-1.05E+00	-1.37E-04	-5.57E-09	-2.49E-04	3.19E-04	-2.77E-05	-1.24E-09	5.89E-06	1.99E-04
1.80E+02	-4.47E-03	-1.05E+00	-1.57E-04	-5.58E-09	-2.49E-04	3.19E-04	-2.77E-05	-1.24E-09	5.87E-06	1.99E-04
2.00E+02	-7.69E-03	-1.05E+00	-2.56E-04	-5.59E-09	-2.50E-04	3.19E-04	-2.76E-05	-1.24E-09	5.88E-06	1.99E-04
2.20E+02	-1.33E-02	-1.06E+00	-6.53E-04	-5.62E-09	-2.53E-04	3.19E-04	-2.73E-05	-1.25E-09	5.90E-06	1.99E-04
2.40E+02	-2.34E-02	-1.07E+00	-2.08E-03	-5.71E-09	-2.86E-04	3.06E-04	-2.55E-05	-1.27E-09	6.04E-06	1.99E-04
2.60E+02	-3.84E-02	-1.08E+00	-6.15E-03	-5.88E-09	-5.20E-04	-4.00E-06	-1.89E-05	-1.31E-09	7.48E-06	1.99E-04
2.80E+02	-3.91E-02	-9.91E-01	-9.72E-03	-5.39E-09	-1.07E-03	-2.07E-03	-3.01E-05	-1.28E-09	1.12E-05	5.91E-04
3.00E+02	8.99E-03	-2.49E-01	1.34E-03	-5.51E-10	-7.25E-06	2.48E-03	7.09E-06	5.50E-10	5.51E-06	6.05E-04
3.20E+02	3.23E-02	2.16E-02	5.31E-03	2.22E-10	2.71E-04	7.60E-04	-3.39E-06	6.83E-11	-1.01E-06	8.01E-07
3.40E+02	2.43E-02	1.76E-02	2.27E-03	1.58E-10	5.45E-05	3.66E-05	-2.46E-06	3.54E-11	-1.99E-07	1.11E-07
3.60E+02	1.55E-02	8.07E-03	6.87E-04	6.96E-11	8.41E-06	1.79E-06	-4.29E-07	1.61E-11	-9.86E-09	7.87E-10
3.80E+02	9.85E-03	3.56E-03	1.73E-04	3.06E-11	1.41E-06	3.11E-07	-5.63E-08	7.63E-12	2.28E-09	-6.38E-08
4.00E+02	6.42E-03	1.65E-03	2.43E-05	1.47E-11	3.23E-07	1.75E-07	-8.03E-09	3.95E-12	-7.21E-09	3.19E-08

z	a1	a2	a3	a4	a5	a6	a7	a8	a9	a10
0.00E+00	-5.00E-04	-5.12E-08	-1.54E-04	-9.57E-06	2.49E-04	5.55E-11	-2.77E-05	-5.61E-09	-5.88E-06	4.81E-11
2.00E+01	-4.80E-04	-5.12E-08	-1.54E-04	-9.60E-06	2.49E-04	5.56E-11	-2.77E-05	-5.81E-09	-5.88E-06	4.81E-11
4.00E+01	-4.16E-04	-5.12E-08	-1.53E-04	-9.71E-06	2.49E-04	5.58E-11	-2.77E-05	-5.78E-09	-5.88E-06	4.82E-11
6.00E+01	-2.96E-04	-5.12E-08	-1.52E-04	-9.92E-06	2.49E-04	5.60E-11	-2.77E-05	-6.37E-09	-5.88E-06	4.84E-11
8.00E+01	-1.02E-04	-5.12E-08	-1.49E-04	-1.03E-05	2.49E-04	5.65E-11	-2.77E-05	-5.58E-09	-5.88E-06	4.86E-11
1.00E+02	2.01E-04	-5.12E-08	-1.46E-04	-1.10E-05	2.49E-04	5.73E-11	-2.77E-05	-5.58E-09	-5.88E-06	4.90E-11
1.20E+02	6.71E-04	-5.12E-08	-1.42E-04	-1.22E-05	2.49E-04	5.85E-11	-2.77E-05	-5.37E-09	-5.88E-06	4.96E-11
1.40E+02	1.40E-03	-5.11E-08	-1.37E-04	-1.44E-05	2.49E-04	6.03E-11	-2.77E-05	-5.39E-09	-5.88E-06	5.05E-11
1.60E+02	2.57E-03	-5.11E-08	-1.37E-04	-1.81E-05	2.49E-04	6.31E-11	-2.77E-05	-1.33E-08	-5.89E-06	5.19E-11
1.80E+02	4.47E-03	-5.12E-08	-1.57E-04	-2.44E-05	2.49E-04	6.75E-11	-2.77E-05	6.39E-09	-5.87E-06	5.41E-11
2.00E+02	7.69E-03	-5.12E-08	-2.56E-04	-3.41E-05	2.50E-04	7.43E-11	-2.76E-05	2.54E-09	-5.88E-06	5.76E-11
2.20E+02	1.33E-02	-5.13E-08	-6.53E-04	-4.66E-05	2.53E-04	8.42E-11	-2.73E-05	1.19E-08	-5.90E-06	6.29E-11
2.40E+02	2.34E-02	-5.17E-08	-2.08E-03	-5.75E-05	2.86E-04	9.41E-11	-2.55E-05	-1.31E-08	-6.04E-06	6.97E-11
2.60E+02	3.84E-02	-5.22E-08	-6.15E-03	-5.64E-05	5.20E-04	5.55E-11	-1.89E-05	-2.04E-09	-7.48E-06	7.36E-11
2.80E+02	3.91E-02	-4.77E-08	-9.72E-03	-3.48E-05	1.07E-03	-2.55E-10	-3.01E-05	1.30E-08	-1.12E-05	1.60E-10
3.00E+02	-8.99E-03	-1.22E-08	1.34E-03	7.52E-07	7.25E-06	3.54E-10	7.09E-06	-3.02E-10	-5.51E-06	1.42E-10
3.20E+02	-3.23E-02	6.22E-10	5.31E-03	2.95E-05	-2.71E-04	7.27E-11	-3.39E-06	3.55E-09	1.01E-06	-2.00E-11
3.40E+02	-2.43E-02	5.65E-10	2.27E-03	3.90E-05	-5.45E-05	-3.39E-11	-2.46E-06	-7.87E-09	1.99E-07	-2.09E-11
3.60E+02	-1.55E-02	2.21E-10	6.87E-04	3.39E-05	-8.41E-06	-3.09E-11	-4.29E-07	-1.04E-08	9.85E-09	-1.61E-11
3.80E+02	-9.85E-03	6.86E-11	1.73E-04	2.41E-05	-1.41E-06	-2.21E-11	-5.63E-08	-1.75E-08	-2.29E-09	-1.13E-11
4.00E+02	-6.42E-03	1.37E-11	2.43E-05	1.53E-05	-3.23E-07	-1.53E-11	-8.05E-09	1.12E-09	7.21E-09	-7.75E-12

As indicated from the table due to the symmetry, the odd harmonics have the same amplitude for the normal and skew terms.

Shielding of the 3x3 array with ferromagnetic shield

First we will check if the shield in the 3D model is as effective in reducing the stray field in the radial direction and see how much flux is going in the axial direction. Then we will build a model with the shield around the array and will explore if flux containment is adequate and if the error field remains within allowable.

Let's introduce a ferromagnetic shield at the radius of 226 mm. The shield length is 600 mm – same as the coils. At this point we do not add anything at the ends to stop the flux in axial direction.

We want to see how bad the problem is and how quick the field decays on its own. We expect there will be some field leakage in the axial direction and possibly in radial direction near the ends.

Assume steel 1010 magnetization curve, which is given in the Table 4.

Table 4. B-H magnetization curve for the 1010 low carbon steel

B, G	H, Oe
0	0
2500.000	2.010619
5000.000	2.613805
9000.000	4.322832
13000.00	9.047787
14500.00	14.07434
15520.00	22.11681
16030.00	32.16991
16550.00	45.23893
16860.00	55.29203
17170.00	67.85841
17690.00	85.45132
18330.00	130.6903
19210.00	211.1150
20450.00	452.3893
21400.00	904.7787
22800.00	2010.619

The field on cylindrical surface at a radius 240 mm is shown in Fig. 32.

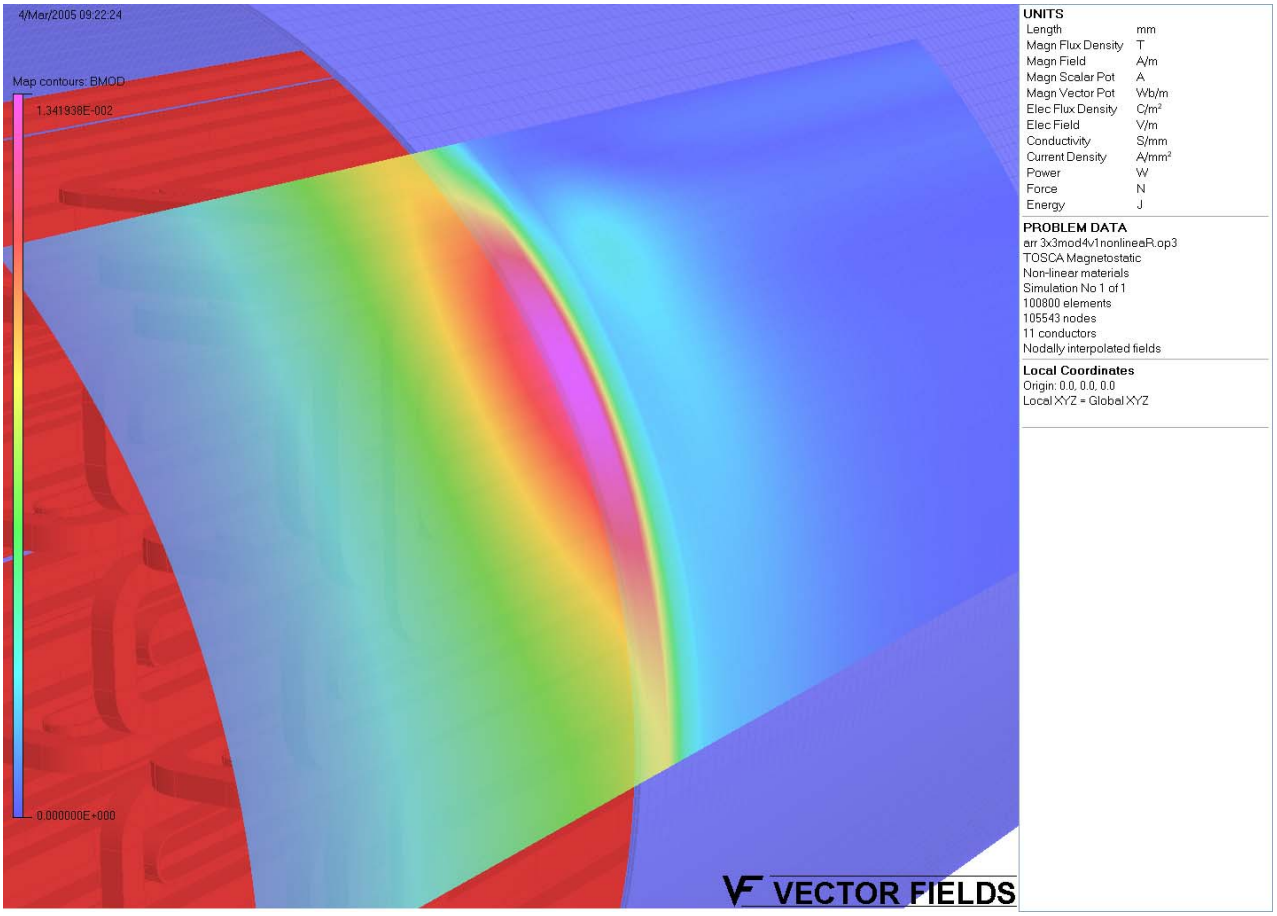

Fig. 32. Stray field is shown on the cylinder at the radius 240 mm – 14 mm away from the shield.

It is seen that the field spills out from the edge of the shield, no surprise. The peak field is 13. 2 mT (132 Gauss) and obviously needs to be shielded better.

In the z direction the flux spills more significantly.

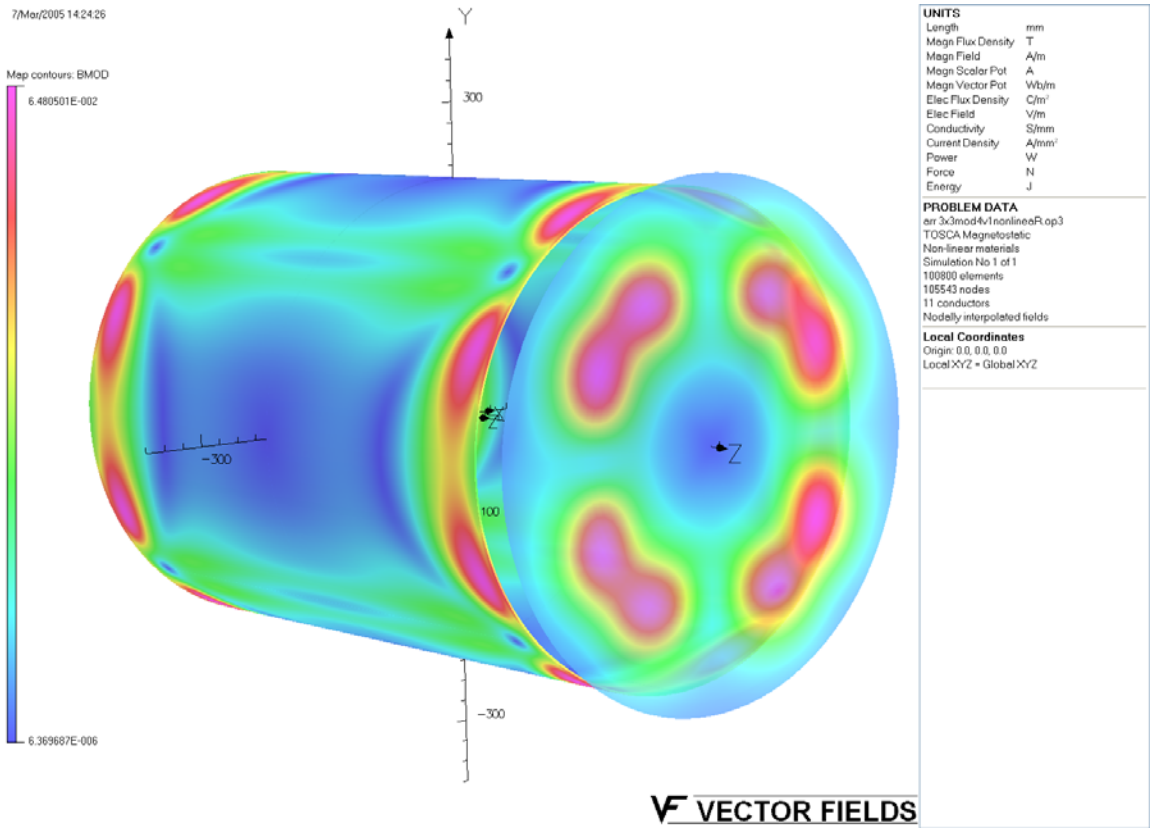

Fig. 33. Stray field on the shield (steel cylinder with R= 226 mm) and on the imaginary disk with R=240 mm at z= 350 mm.

Fig. 33 shows the field on the disk with R=240mm at z= 350 mm, 50 mm from the coils end. We see that the stray field is about 650 G and needs to be shielded. Fig. 33 also shows field distribution on the shielding cylinder.

In our next step we enclose the array with a 4 mm thick iron shield. We leave only 60 mm diameter holes for the beams and will explore the stray field and changes in the error fields. In practice it may be a special shield or it can be a vacuum vessel to contain the flux.

We enclose the windings with a 4 mm thick steel shield at the radius 226 mm (diagonal of 160 mm square). In the end region we will put a flange at z=315 mm (15 mm away from the winding ends. The holes in the flange are 60 mm in diameter.

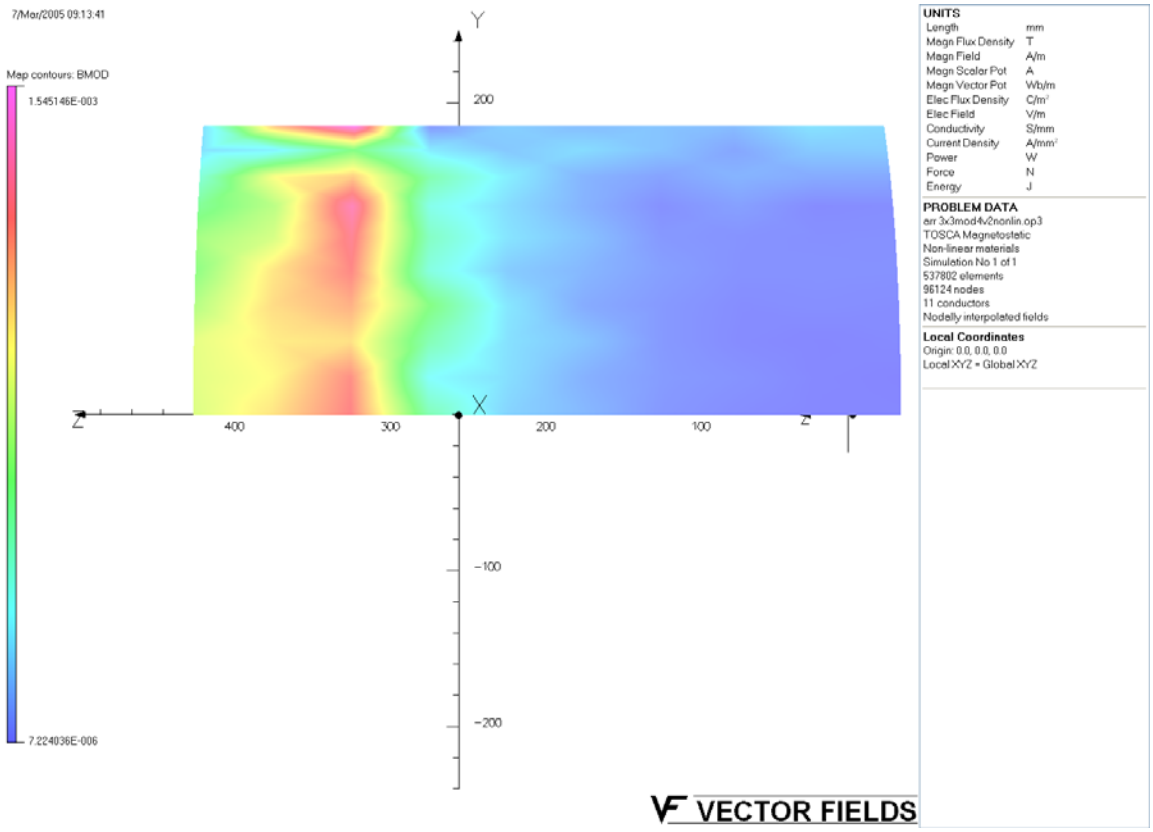

Fig. 34. Stray field on the cylinder with R=240 mm.

Fig. 34 shows the field on the 240 mm radius cylinder. The peak field is 15 G, which may already be acceptable. If not – the shield could be made thicker.

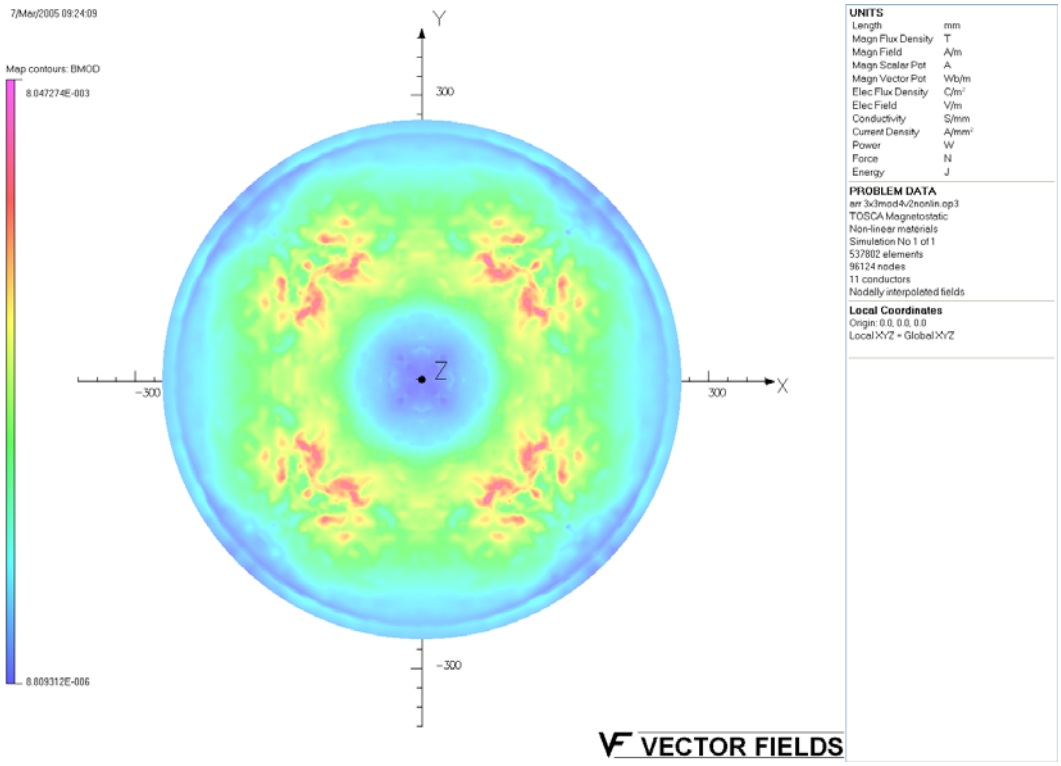

Fig. 35.Field on a 240 mm radius disk, 350 mm from the center (50 mm away from the end of the coils, 30 mm away from the shield.

Fig. 35 shows that although there are some 80 G islands, at the periphery the field is very low and may be already acceptable.

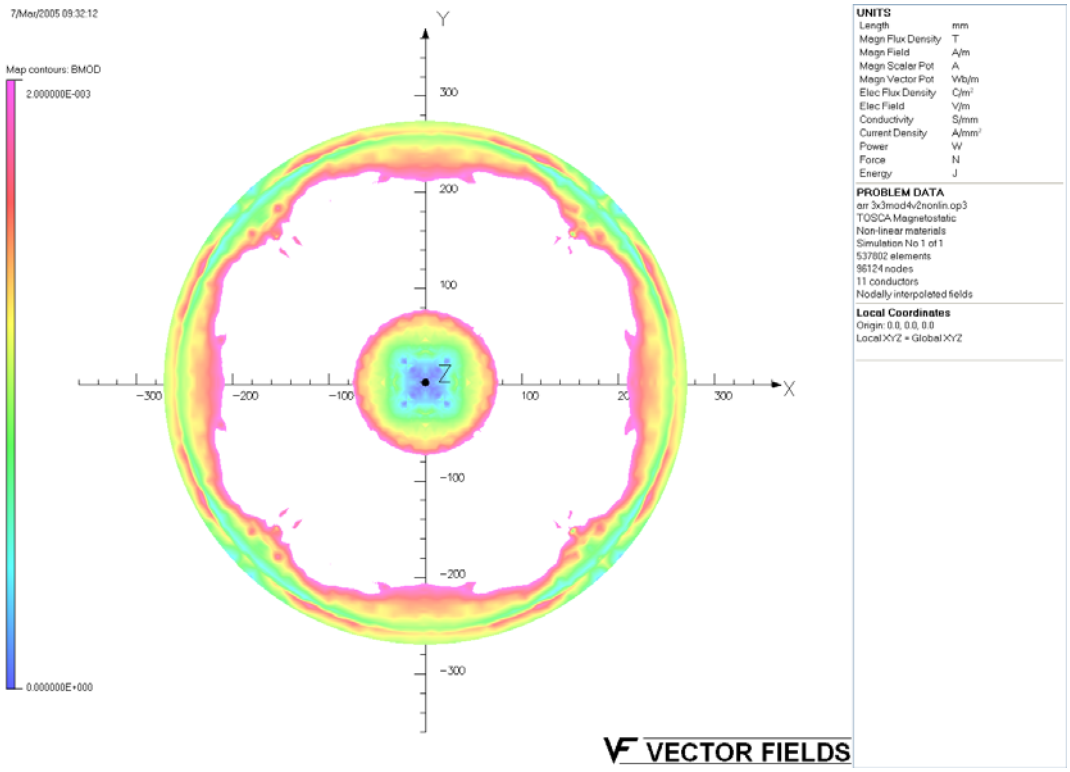

Fig. 36. Magnetic field at the periphery of the disk shown in Fig. 35. Area with no color on the disk corresponds to fields higher than 20 G.

The same field map with max 20 G, is presented in Fig. 36, showing that the stray field is low at the edges of the 240mm radius disk.

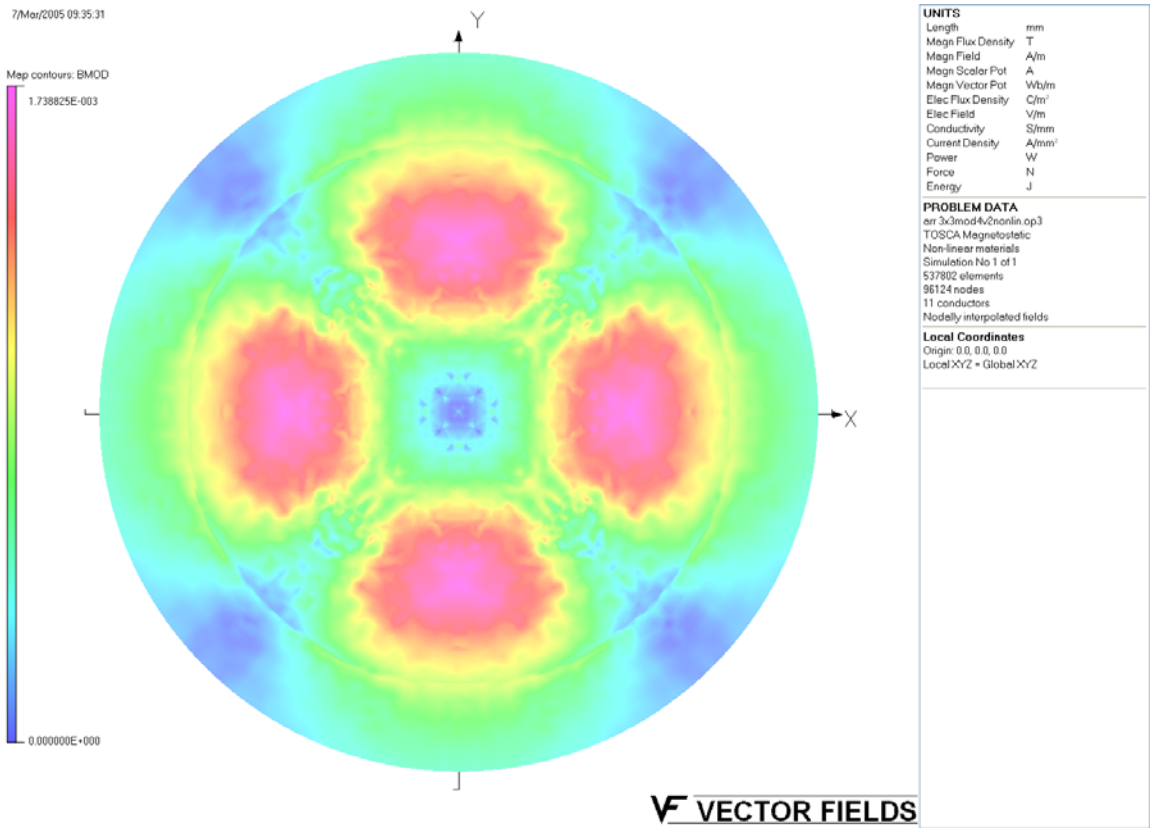

Fig. 37. Field map on a disk at z=400 mm, 100 mm away from the

Fig. 37 shows how stray field looks on a 400 mm radius disk 400 mm away from the center (100 mm away from the coil ends, 80 mm away from the shield).

Field on the surface of the shield (see Fig. 38) shows that the flange is in condition close to saturation. If necessary, another layer of shielding could be used to further reduce the stray field lower.

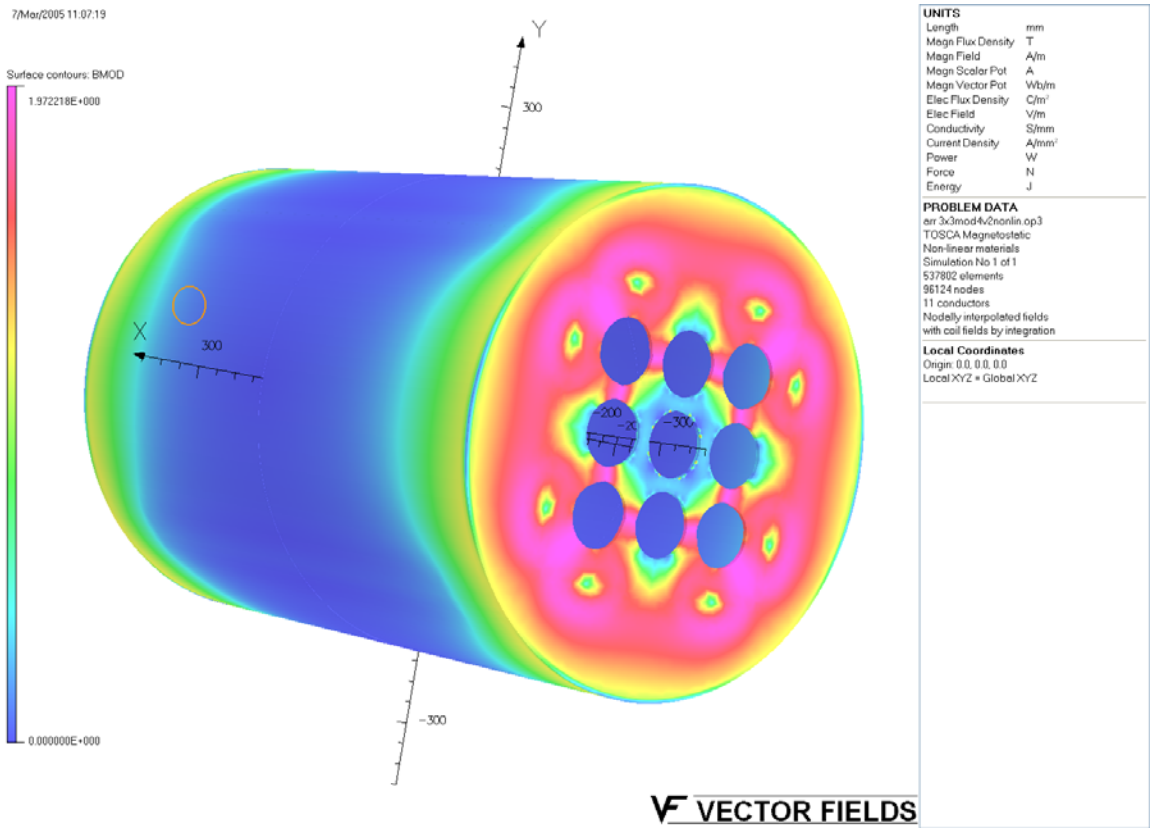

Fig. 38. Magnetic field on the surface of the shield.

Thus, our studies show that a low carbon steel shield is very effective in containing the stray field. The radial field was low from the start, as expected. If it is necessary to reduce the axial field, additional thickness or better an additional shield could be used in the axial direction.

Effect of the shield on the error field in the array

Fig. 39-41 show error fields in the cells with the shield and compare them with the unshielded version.

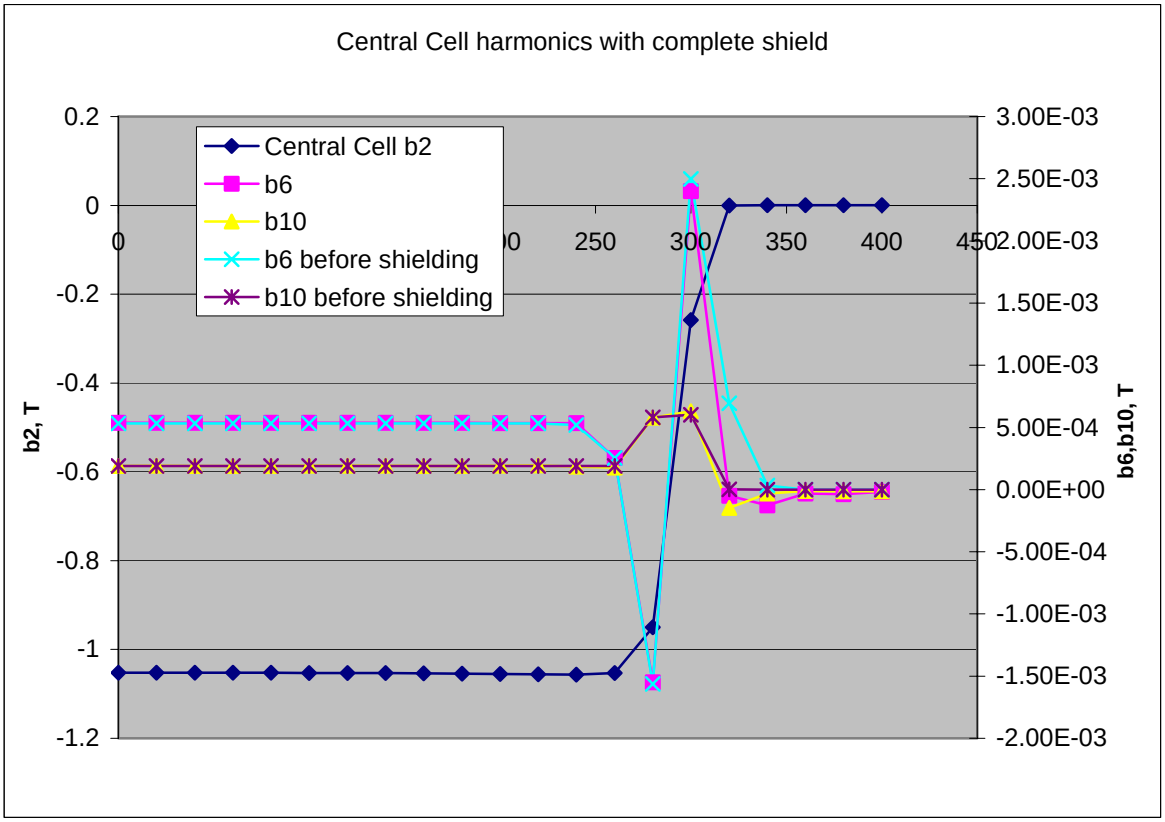

Fig. 39. Error field in the central cell in the completely shielded 3x3 array compared with the error fields before the shielding

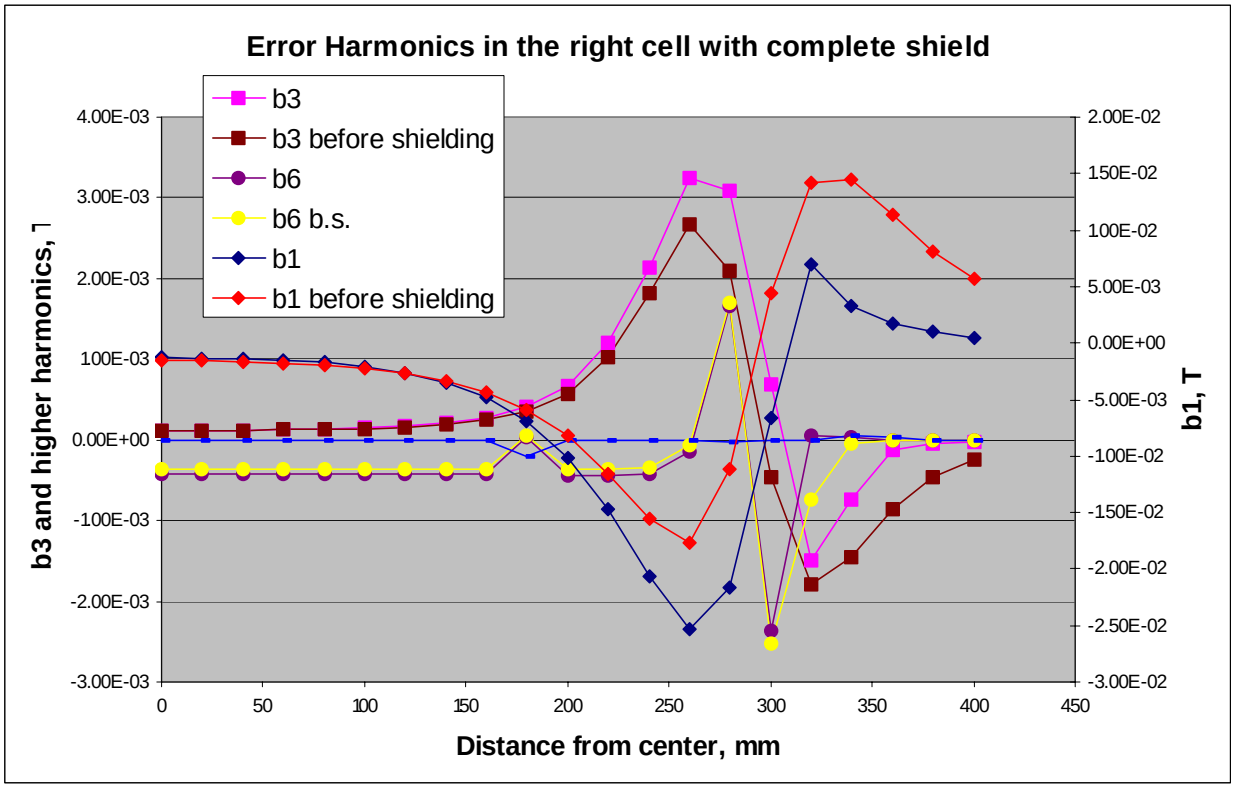

Fig. 40. Selected harmonics of the error field in the shielded version of Model 4 in comparison with the Model 4 without the shield.

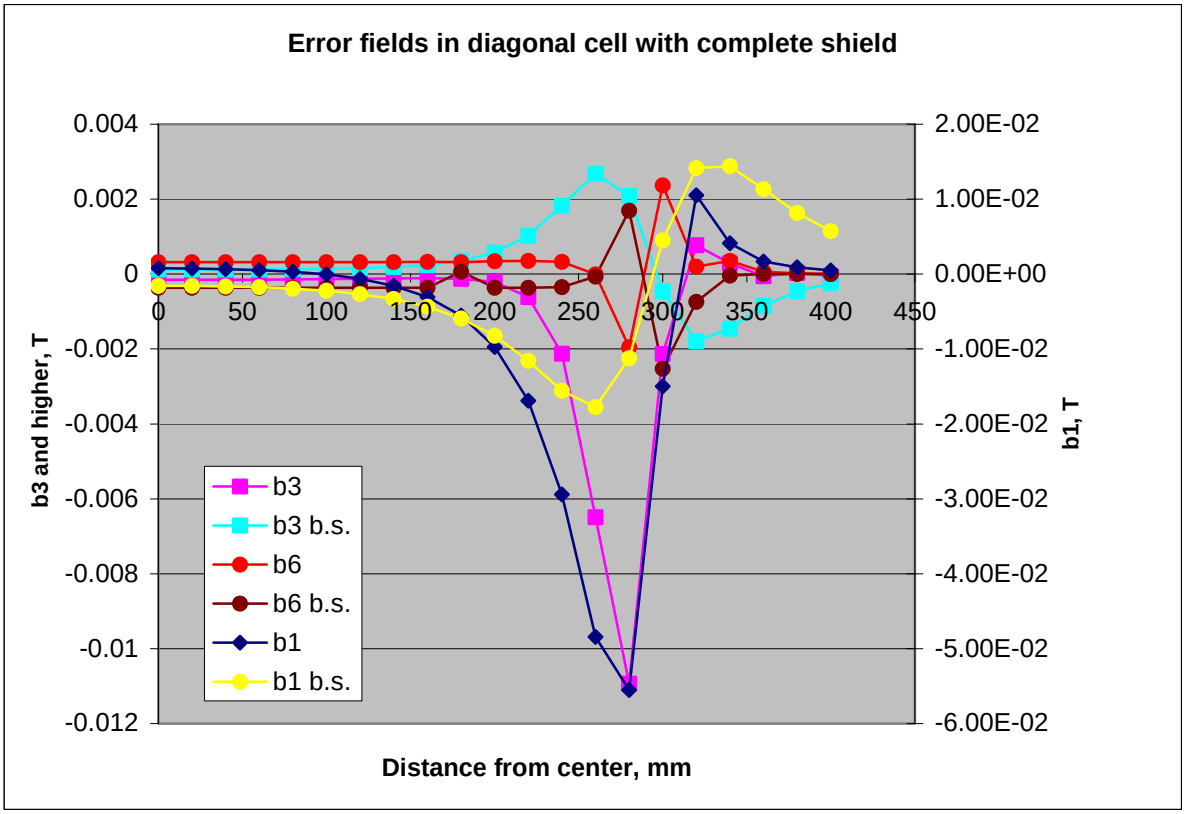

Fig. 41. Selected harmonics in the diagonal cell with and without shielding.

We can see that the field harmonics in the central and the right bores changed insignificantly in comparison with Model 4 without the shield. The diagonal cell showed much bigger effect of the shield on the field quality for the worse, especially, component b3, which may require some improvement, but this effort is outside the scope of this report.

This is understandable, since the diagonal cell is close to the shield while the other cells are farther away. This effect is purely the end effect and could be corrected either by modification of the ends or compensated by the straight runs to give an integrated error field small.

Conclusions

We have found a practical solution for 3x3 focusing array for a HIF driver, that meets all specifications, Model 4 and its modification Model 4A. We showed that shielding could be achieved with a thin ferromagnetic shield.

Although some more optimization may be desirable, we showed that there are no showstoppers in development and building such an array. Since the proposed solution is not particularly specific to 3x3 array, the proposed principle could be used for an arbitrary size array for HIF.

Since this solution is the first practical proposal for a low error field focusing arrays, it is an essential step in proving the feasibility of a multi-beam induction accelerator in particular for heavy ion driver for inertial confinement fusion .

Acknowledgement

I am grateful to Maxim Umansky for his cross checking of my computations and useful discussions.

References

[1] N. Martovetsky, Array shielding with racetrack magnets, Memorandum, LLNL, 1/31/03.

[2] A. Faltens, D. Shuman, A Superconducting Quadrupole Array for Transport of Multipole High Current Beams", IEEE NPSS, October 25-29, 1999, SOFE 99, p. 362-365.

[3] C. Gung, J.V. Minervini, J.H. Schultz, N.N. Martovetsky, R.R. Manahan, G. Sabbi, P.A. Seidl Construction and Tests of HCX Quadrupole Doublet for Heavy Ion Beam Transport Experiments, presented at ASC 2004 conference in Jacksonville, Fl.

[4] R. Meinke, Field uniformity optimization of a 3x3 quadrupole array, Feb. 28, 2005, presentation at the conference call, unpublished